iScience

CellPress
OPEN ACCESS

Article

Integrative analysis of metabolome and transcriptome reveals a dynamic regulatory network of potato tuber pigmentation

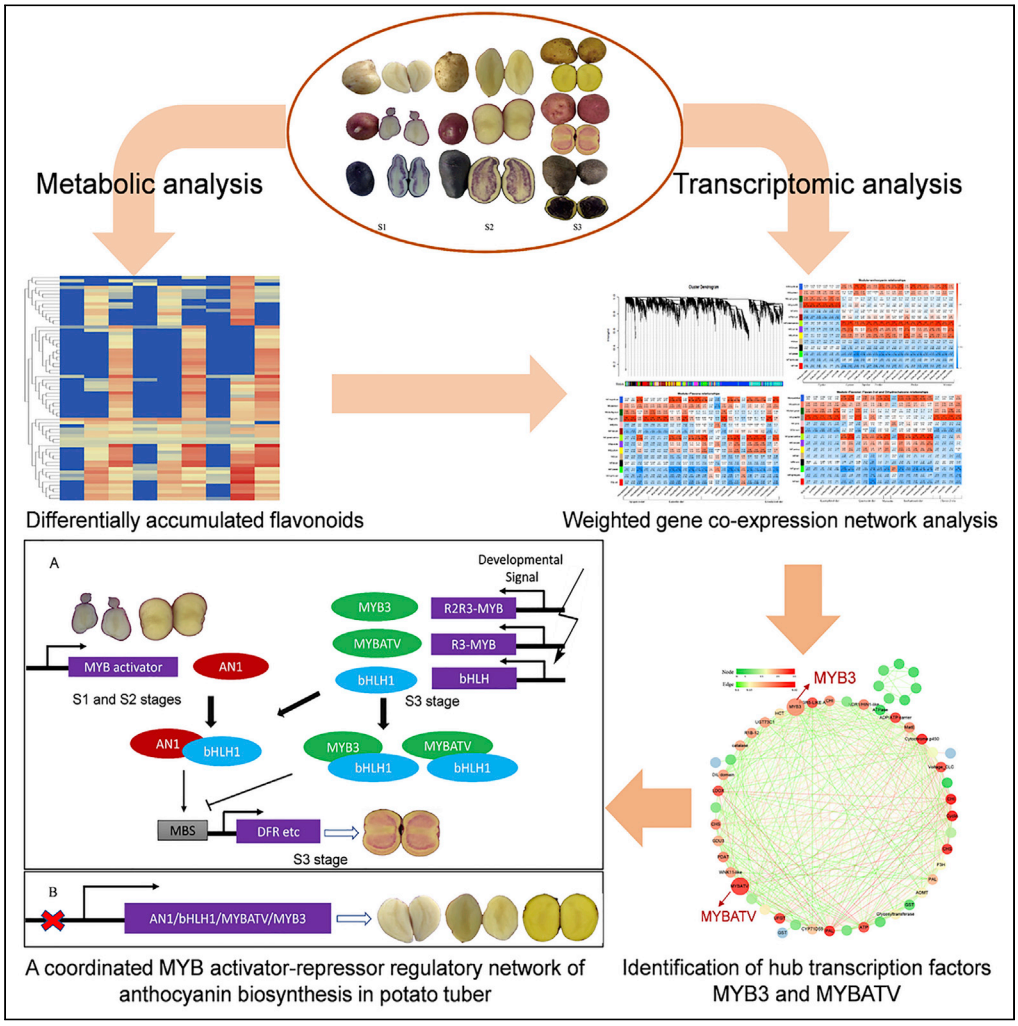

Yuhui Liu, Yuanming Li, Zhen Liu, ..., Chao Sun, Junlian Zhang, Jiangping Bai

baijp@gsau.edu.cn

Highlights

Seventy-two flavonoids were identified in differentially pigmented potato tuber

Candidate genes for flavonoid biosynthesis were identified

Two MYB repressors play roles in a feedback regulatory network on tuber pigmentation

Liu et al., iScience 26, 105903
February 17, 2023
https://doi.org/10.1016/j.isci.2022.105903

iScience

CellPress
OPEN ACCESS

Article

Integrative analysis of metabolome and transcriptome reveals a dynamic regulatory network of potato tuber pigmentation

Yuhui Liu,[1,5] Yuanming Li,[2,5] Zhen Liu,[1] Lei Wang,[3] Kui Lin-Wang,[4] Jinyong Zhu,[1] Zhenzhen Bi,[1] Chao Sun,[1] Junlian Zhang,[1,2] and Jiangping Bai[1,6,*]

SUMMARY

Potatoes consist of flavonoids that provide health benefits for human consumers. To learn more about how potato tuber flavonoid accumulation and flesh pigmentation are controlled, we analyzed the transcriptomic and metabolomic profile of potato tubers from three colored potato clones at three developmental phases using an integrated approach. From the 72 flavonoids identified in pigmented flesh, differential abundance was noted for anthocyanins, flavonols, and flavones. Weighted gene co-expression network analysis further allowed modules and candidate genes that positively or negatively regulate flavonoid biosynthesis to be identified. Furthermore, an R2R3-MYB repressor StMYB3 and an R3-MYB repressor StMYBATV involved in the modulation of anthocyanin biosynthesis during tuber development were identified. Both StMYB3 and StMYBATV could interact with the cofactor StbHLH1 and repress anthocyanin biosynthesis. Our results indicate a feedback regulatory mechanism of a coordinated MYB activator-repressor network on fine-tuning of potato tuber pigmentation during tuber development.

INTRODUCTION

With potato (*Solanum tuberosum* L.) being a major staple crop around the world, the pigmented cultivars have attracted research interest because of substantial anthocyanin accumulation, giving both specialty and capacity for nutritional benefits to human health.[1,2] Anthocyanins are classified within the flavonoid group of compounds, which are derived from the well-characterized flavonoid biosynthetic pathway in many plants.[3] Flavonols, flavones, isoflavones, flavanones, anthocyanins, and condensed tannins (proanthocyanidins, PAs) are among the final products of flavonoid biosynthesis, which starts with phenylalanine.[3] The phenylalanine is then converted into *p*-coumaroyl-CoA, with the reaction catalyzed by phenylalanine ammonia-lyase (PAL), 4-coumarate-CoA ligase (4CL), and cinnamic acid hydroxylase (C4H). Through a condensation reaction, chalcone synthase (CHS) then converts *p*-coumaroyl-CoA and fatty acid-derived malonyl CoA into naringenin chalcone which is subsequently catalyzed by different enzymes within the pathway to yield various flavonoid compounds. Of these, flavanone 3-hydroxylase (F3H), flavonoid 3′5′-hydroxylase (F3′5′H), flavonoid 3′-hydroxylase (F3′H), and dihydroflavonol 4-reductase (DFR) direct the route toward leucoanthocyanins. The colorless leucoanthocyanins are then converted by anthocyanidin synthase (ANS/LDOX) to colored anthocyanidins such as cyanidin, delphinidin, and pelargonidin prior to glycosylation by Uridine 5′-diphosphate (UDP)-glucose flavonoid-*O*-glycosyl transferase (UFGT) or other chemical modifications such as methylation and acylation. These products are transported from the cytosol to vacuoles for storage via different types of mechanisms mediated by the glutathione S-transferases (GST), ATP binding cassette (ABC) proteins, and multidrug and toxic extrusion (MATE).[4–6] Other enzymes involved in the manufacture of flavonols, flavones, isoflavones, and PAs include flavonol synthase (FLS), flavone synthase (FNS), isoflavone synthase (IFS), anthocyanin reductase (ANR), and leucoanthocyanidin reductase (LAR).[3,7,8]

In addition to genes encoding flavonoid-related enzymes, transcription factors (TFs) that influence gene expression have been found in various species. For instance, gene expression within this pathway is

[1]State Key Laboratory of Aridland Crop Science/Agronomy College, Gansu Agricultural University, Lanzhou 730070, China

[2]College of Horticulture, Gansu Agricultural University, Lanzhou 730070, China

[3]Potato Research Center, Hebei North University, Zhangjiakou 075000, China

[4]The New Zealand Institute for Plant and Food Research Limited, Mt Albert, Private Bag 92169, Auckland Mail Centre, Auckland 1142, New Zealand

[5]These authors contributed equally

[6]Lead contact

*Correspondence: baijp@gsau.edu.cn

https://doi.org/10.1016/j.isci.2022.105903

controlled by the MYB-bHLH-WD40 (MBW) complex which basically involves interactions between MYB, the basic-helix-loop-helix (bHLH), and the WD40/WDR regulators.[9,10] Within the flavonoid pathway, the different branches that yield separate end compounds are separately regulated by different MYB TFs (mainly R2R3-MYB), leading to flavonol, PAs, and anthocyanins,[11,12] with 13 out of 126 R2R3-MYB members controlling flavonoid metabolism in the case of *Arabidopsis*.[13] Flavonol biosynthesis requires regulation by MYB11, MYB12, and MYB111 of the R2R3-MYB group of TFs,[14] while in the seed coat of *Arabidopsis*, the accumulation of PAs is regulated by a minimum of four MBW complexes TT2(MYB123)-TT8/GL3/EGL3(bHLH)-TTG1(WD40), MYB5-TT8-TTG1 with partially overlapped functions.[15] The R2R3-MYB activators which take part in the process of anthocyanin synthesis are well characterized in many species, with some examples being *VvMYBA2* and *VvMYBA1* in grapevine (*Vitis vinifera*) berries,[16] *StAN1* in potato (*S. tuberosum*),[17,18] and *AtMYB114*, *AtMYB113*, *AtMYB90/PAP2*, and *AtMYB75/PAP1* in *Arabidopsis*[19] as well as *MdMYB110a*, *MdMYB10*, *MdMYBA*, and *MdMYB1* in apples (*Malus* × *domestica*).[20,21] Similarly, in *Arabidopsis*, R2R3-MYB and R3-MYB repressors such as *AtMYB3/4/6* and *CAPRICE (CPC)/TRIPTYCHON (TRY)/AtMYBL2* are also recognized.[22,23]

Other TFs such as MADS-box,[24] zinc finger proteins,[25] AP2/ERF,[26] the WRKY family,[27,28] and the bZIP family[29,30] also highlight the significance of transcriptional regulation for controlling flavonoid biosynthesis. They mostly co-regulate flavonoid production by interacting with members of the MBW complex; for example, AP2/ERF TFs complexed with PyMYB114 to positively co-regulate anthocyanin accumulation in pear (*Pyrus bretschneideri*),[31] while in red-fleshed apple, the MdHY5-MdWRKY41-MdMYB complex influences the synthesis of anthocyanin and PAs.[28] Other transcription factors are also recognized as upregulating key R2R3 MYB controllers. For example, several peach NAC [No apical meristem (**NAM**), Arabidopsis transcription activation factor (**ATAF**), Cup-shaped cotyledon (**CUC**)] TFs upregulate peach *MYB10* expression in red-fleshed peaches (*Prunus persica*).[32]

Characterizing the flavonoid biosynthesis pathway in potatoes as well as associated regulatory genes has been the focus of several studies.[17,18,33–43] In the present work, we examined potato clones developed by conventional breeding procedures from the same ancestor, which showed yellow, red, and purple pigmentation. This feature allows the identification of factors responsible for flavonoid biosynthesis without confounding the genetic background. Joint transcriptome and metabolome analyses identified potato tubers' major flavonoid compounds and corresponding genes. A total of 72 flavonoids were placed, and weighted gene co-expression network analysis (WGCNA) provided co-expressed gene modules that allowed genes which are essential for controlling flavonoid synthesis to be identified. Two MYB repressors (an R2R3-MYB and an R3-MYB) were determined engaged in feedback regulatory mechanisms underlying the biosynthesis of flavonoid accumulation in colored potatoes during tuber development. The current study will clarify the temporal accumulation of flavonoids in different colored potato tubers, expand our understanding of the regulatory mechanism of flavonoid synthesis, and facilitate research into engineering flavonoid composition in potato tubers.

RESULTS

Metabolic differences between the three potato clones over development

Seventy-two types of flavonoids were detected in three potato clones at different developmental stages (Figure 1A) including 24 anthocyanins, 21 flavones, 18 flavonols, four flavan-3-ols, two dihydroflavones, one dihydrochalcone, one dihydroflavonol, and one isoflavone (Table 1). We screened differentially accumulated flavonoids (DAFs) using a |Log2 (fold change)| $\geq$ 1, a variable importance in project (VIP) value of $\geq$1, and a p value <0.05 as thresholds. The numbers of DAF ranged from 31 to 56, 27 to 51, and 42 to 62 between two potato clones at three developmental stages (S1, S2, and S3) and from 1 to 3, 15 to 40, and 9 to 32 between two developmental stages of Y, R, and P, respectively (Figures 1B and 1C).

Ten flavonoids were ubiquitously accumulated in the flesh of R and P tubers, even when the tuber flesh of R was white or yellow at S1 and S2, with most of these flavonoids being pelargonidin (Pg) derivatives. Forty-seven flavonoids were accumulated in purple flesh of P at three stages, of which 20 flavonoids were exclusively reserved in purple flesh: two malvidin (Mv) derivatives, nine petunidin (Pt) derivatives, one delphinidin (Dp), one cyanidin (Cy) derivative, four flavonols, two flavones, and one isoflavone (Figure S1 and Table S2). Twenty-three flavonoids accumulated in white, yellow, and red flesh of R at three stages, in which seven flavonoids were specifically accumulated: five flavones and two flavan-3-ols. The numbers of common and unique flavonoids in different clones at different developmental stages are

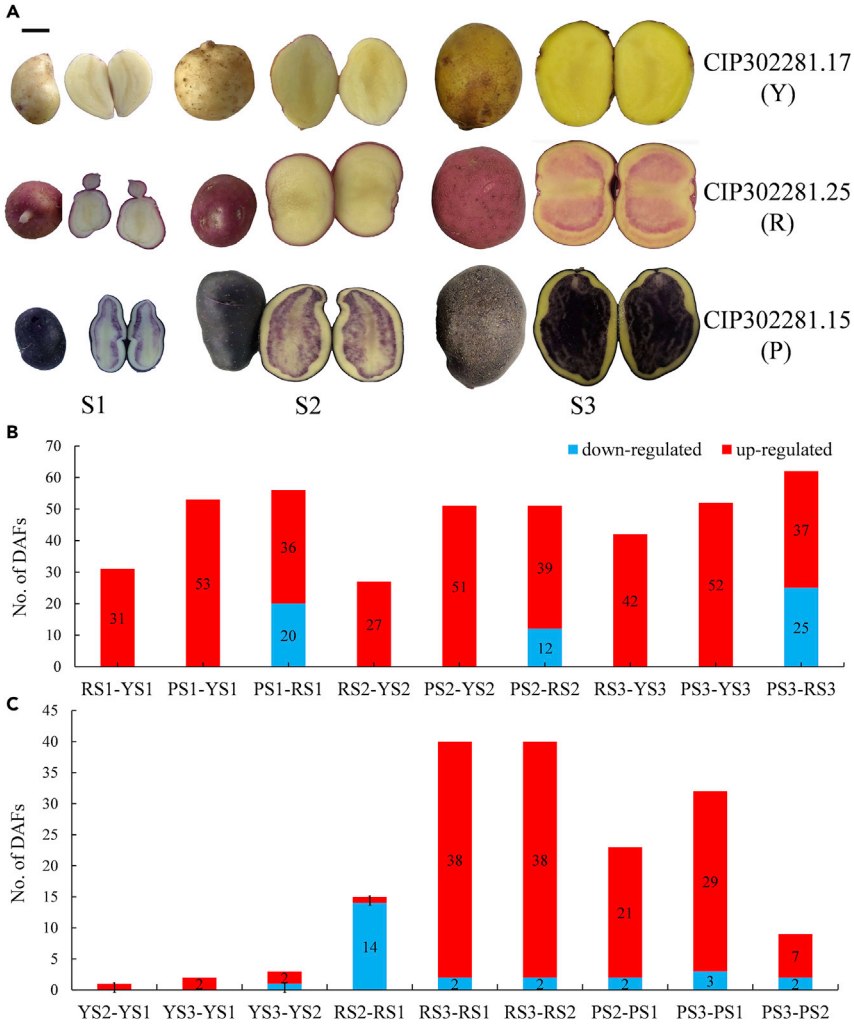

Figure 1. Tuber color and number of differentially accumulated flavonoids among three potato clones at three developmental stages

(A) Tuber colors of three potato clones at three developmental stages, CIP 302281.17, CIP 302281.25, and CIP 302281.15, were renamed as Y, R, and P according to their dominant flesh color. S1, S2, and S3 represent tuberization, tuber bulking, and tuber maturation stages, respectively. Scale bar, 1 cm.

(B) Numbers of differentially accumulated flavonoids (DAFs) among Y, R, and P at three stages.

(C) Numbers of DAFs among three developmental stages. See also Table 1 and Figure S1.

shown in Venn diagrams in Figures S1A and S1B. Twenty-four flavonoids were present in red and purple tuber flesh, in which nine flavonoids were exclusively accumulated: one Dp derivative, five flavones, two flavonols, and one dihydroflavone (Figure S1A and Table S2). We further identified 40 DAFs between white/yellow flesh and red flesh of R, of which 13 flavonoids showed uniquely significant accumulation in red flesh with $|Log_2(\text{fold change})|$ from 1.62 to 12.25: five anthocyanins (Pg, Dp, and Cy derivatives), two flavan-3-ols, four flavonols, and two flavones (Figure S1B and Table S2).

The composition or general structure of flavonoid compounds differed depending on the potato cultivar and developmental stage, indicating that the pigmentation of potato tubers could be influenced by these metabolites. Several kaempferol, apigenin, dihydrokaempferol, eriodictyol, and quercetin derivatives and all the six Pg derivatives were more abundant in red flesh. The common monomeric precursors (flavan-3-ols) of the proanthocyanidins—afzelechin and epiafzelechin—showed high accumulation in the red flesh of the red clone at S3. The accumulation of Pn, Cy, Mv, Pt, and Dp led to the dark purple appearance of

Table 1. Flavonoid metabolites detected in three potato clones

Metabolite Index	Compounds	Q1 (Da)	Molecular Weight (Da)	Formula	Ionization model	YS1[a]	RS1[a]	PS1[a]	YS2[a]	RS2[a]	PS2[a]	YS3[a]	RS3[a]	PS3[a]
1.Hmmp001656	Pelargonin-*O*-rutinoside	579	578	C27H31O14	[M + H]+	9	112000	47833	9	58633	39767	9	1038000	31633
2.Hmmp001174	Pelargonin-*O*-Hexoside-*O*-rhamnoside-*O*-Hexoside	741	740	C33H41O19	[M + H]+	9	133000	35467	9	53467	103733	9	1063333	59333
3.Zmmp001791	Pelargonidin-3-rutinoside-5-glucoside	741	741	C33H41O19+	[M]+	9	60867	18533	9	27133	55233	9	583000	32567
4.Zmmp003570	Pelargonidin3-*p*-coumaroylrutinoside-5-glucoside	887	887	C42H47O21+	[M]+	9	171000	56767	9	107500	93467	9	5163333	106900
5.Zmmp003304	Pelargonidin 3-*O*-[2-*O*-Glucosyl-6-*O*-*p*-Coumaroyl-Glucoside]-5-*O*-(Glucoside)	903	903	C42H47O22+	[M]+	9	4300	2733	9	3017	679	9	144333	4717
6.pme3392	Pelargonidin 3-*O*-glucoside	433	433	C21H21O10+	[M]+	9	82233	20400	9	48167	8877	9	693667	14633
7. pmb0550	Cyanidin 3-*O*-glucoside (Kuromanin)	449	449	C21H21O11+	[M]+	9	4886	26800	9	9	30833	9	9	26467
8.pme1773	Cyanidin 3-*O*-rutinoside (Keracyanin)	595	595	C27H31O15+	[M]+	9	110333	1700000	9	81633	2363333	9	251333	1286667
9.Zmmp003451	Cyanidin-3-*p*-coumaroylrutinoside-5-glucoside	903	903	C42H47O22+	[M]+	9	3043	110333	9	9	235333	9	155667	463667
10.Zmmp003244	Delphinidin-3-*p*-coumaroylrutinoside-5-glucoside	919	919	C42H47O23+	[M]+	9	9	55100	9	9	139667	9	9	357000
11.pme3256	Delphinidin 3-*O*-rutinoside	611	611	C27H31O16+	[M]+	9	9	1066667	9	9	1356667	9	5187	877667
12.Zmmp003722	Peonidin-3-feruloylrutinoside-5-glucoside	947	947	C44H51O23+	[M]+	9	3830	67233	9	9	115667	9	11733	74100
13.Zmmp003631	Peonidin-3-*p*-coumaroylrutinoside-5-glucoside	917	917	C43H49O22+	[M]+	9	9917	347667	9	1123	720333	9	114500	921333
14.pme3391	Petunidin 3-*O*-glucoside	479	479	C22H23O12+	[M]+	9	9	10130	9	9	39600	9	9	35433
15.Zmmp003478	Petunidin-3-*p*-coumaroylrhamnoside-5-glucoside	771	771	C37H39O18+	[M]+	9	646	129333	436	9	224333	9	2189	273333
16.Zmmp003779	Petunidin-3-*p*-coumaroylrutinoside	771	771	C37H39O18+	[M]+	9	9	146333	9	9	173000	9	9	368333
17.Zmmp001564	Petunidin-3-rutinoside-5-glucoside	787	787	C34H43O21+	[M]+	9	9	149333	9	9	597667	9	9	244000
18.Zmmp004046	Petunidin-3-*p*-coumaroylrutinoside-5-glucoside	933	933	C43H49O23+	[M]+	9	9	157667	9	9	298667	9	9	637333
19.Zmmp003482	Petunidin-3-*p*-coumaroylrutinoside-7-glucoside	933	933	C43H49O23+	[M]+	1663	9	1110000	9	9	2096667	826	3539	2780000
20.Zmmp003155	Petunidin-3-caffeoylrutinoside-5-glucoside	949	949	C43H49O24+	[M]+	9	9	77767	9	9	62833	9	9	108200

(*Continued on next page*)

Table 1. *Continued*

Metabolite Index	Compounds	Q1 (Da)	Molecular Weight (Da)	Formula	Ionization model	YS1[a]	RS1[a]	PS1[a]	YS2[a]	RS2[a]	PS2[a]	YS3[a]	RS3[a]	PS3[a]
21.Zmmp003556	Petunidin-3-feruloylrutinoside-7-glucoside	963	963	C44H51O24+	[M]+	9	9	110633	9	9	230667	9	9	168000
22.Zmmp004160	Petunidin-3-feruloylrutinoside-5-glucoside	963	963	C44H51O24+	[M]+	9	9	15033	9	9	28200	9	9	28133
23.Zmmp004296	Malvidin-3-*p*-coumaroylrutinoside-5-glucoside	947	947	C44H51O23+	[M]+	9	9	2483	9	9	13033	9	9	23767
24.Zmmp003756	Malvidin-3-feruloylrutinoside-5-glucoside	977	977	C45H53O24+	[M]+	9	9	8267	9	9	19400	9	9	10493
25.mws2118	Phloretin 2′-*O*-glucoside	435	436	C21H24O10	[M−H]-	1317	4760	13750	898	5590	34233	1111	95133	47367
26.Hmmn002691	Eriodictiol-*O*-Hexoside-*O*-rhamnoside-*O*-Hexoside-*O*-rhamnoside	903	904	C39H52O24	[M−H]-	9	151000	48300	9	41933	41000	174	5836667	50000
27.Hmmn002379	Eriodictiol-*O*-Hexoside-*O*-rhamnoside-*O*-Hexoside-*O*-Hexoside	919	920	C39H52O25	[M−H]-	9	9	132333	9	9	238333	9	133833	500667
28.mws1094	Dihydrokaempferol	287	288	C15H12O6	[M−H]-	9	44600	2150	9	15800	9	9	106567	9
29.mws1422	(−)-Epiafzelechin	275	274	C15H14O5	[M + H]+	9	10120	9	9	8363	9	463	114733	4703
30.mws0034	Epigallocatechin gallate	457	458	C22H18O11	[M−H]-	2236	9	5686	969	9	9	9	234339	1123
31.mws0351	Gallate catechin gallate	457	458	C22H18O11	[M−H]-	9	9	9	8373	9	9	9	144673	9
32.pme3285	Afzelechin(3,5,7,4′-Tetrahydroxyflavan)	275	274	C15H14O5	[M + H]+	9	34400	886	9	23700	756	9	182667	2350
33.Hmmp002447	Apigenin-*O*-rutinoside-*O*-Hexoside	725	724	C33H40O18	[M + H]+	9	5706	9	9	11903	9	9	1230000	9
34.Hmmp002474	Apigenin-*O*-Hexoside-*O*-rhamnoside-*O*-glucuronate	755	754	C33H38O20	[M + H]+	9	49600	9	9	129333	9	9	546000	9
35.Hmmp002073	Apigenin-*O*-Hexoside-*O*-rhamnoside-*O*-Hexoside-*O*-Hexoside	903	902	C39H50O24	[M + H]+	9	7536	300000	9	4483	530667	9	442333	972000
36.Hmmp002266	Apigenin-*O*-Hexoside-*O*-rhamnoside-*O*-rhamnoside-*O*-Hexoside	887	886	C39H50O23	[M + H]+	9	366667	91633	9	177000	188000	3213	10810000	233667
37.pme2459	Luteolin 7-*O*-glucoside(Cynaroside)	449	448	C21H20O11	[M + H]+	9	51633	9	9	32767	9	439	509667	9
38.pmp000593	Luteolin-7-*O*-rutinoside	595	594	C27H30O15	[M + H]+	9	14667	1083	9	4527	439	9	130000	9
39.pmp001079	Luteolin-7-*O*-neohesperidoside(Lonicerin)	595	594	C27H30O15	[M + H]+	9	15267	9	9	5573	9	9	156667	9
40.pmp000595	Luteolin-7,3′-Di-*O*-β-D-Glucoside	611	610	C27H30O16	[M + H]+	9	9	19433	9	9	48100	9	29933	80933
41.Hmpp002612	Luteolin-7-*O*-β-D-gentiobioside	611	610	C27H30O16	[M + H]+	9	9	34567	9	9	57233	9	43933	97933
42.Hmmn003584	Luteolin-*O*-rutinoside-*O*-rhamnoside	739	740	C33H40O19	[M−H]-	9	16033	9	9	4627	9	9	929667	9
43.Hmmp002169	Luteolin-*O*-Hexoside-*O*-rhamnoside-*O*-rhamnoside-*O*-Hexoside	903	902	C39H50O24	[M + H]+	9	8097	369000	9	4683	541000	9	457333	1097333

(*Continued on next page*)

Table 1. *Continued*

Metabolite Index	Compounds	Q1 (Da)	Molecular Weight (Da)	Formula	Ionization model	YS1[a]	RS1[a]	PS1[a]	YS2[a]	RS2[a]	PS2[a]	YS3[a]	RS3[a]	PS3[a]
44.CWJP002289	Luteolin-3-*O*-glucosyl-rhamnosyl-glucoside-glucoside	919	918	C42H46O23	[M + H]+	9	9	179667	9	9	317667	9	1413	932667
45.Zmhp002897	Isochrysoeriol C-hexosyl-*O*-hexoside	625	624	C28H32O16	[M + H]+	9	9	57467	9	9	132333	9	19667	147000
46.mws0043	Nobiletin	403	402	C21H22O8	[M + H]+	4727	4740	5183	4833	4917	4380	4687	4713	4680
47.pmb3041	Tricin O-saccharic acid	521	522	C23H22O14	[M−H]-	109800	210667	260667	162667	338333	176000	87500	48300	57733
48.Zmhp002798	Isosaponarin	595	594	C27H30O15	[M + H]+	9	9	9	9	9	5523	9	299333	7807
49.Hmmp002322	Chrysoerio-*O*-Hexoside-*O*-rhamnoside-*O*-rhamnoside-*O*-Hexoside	917	916	C40H52O24	[M + H]+	9	83067	1170000	1093	113333	2340000	9	1293333	3026667
50.Hmmp002324	Tricin-*O*-Hexoside-*O*-rhamnoside-*O*-rhamnoside-*O*-Hexoside	947	946	C41H54O25	[M + H]+	9	14700	391000	9	10393	716000	9	22703	628000
51.mws0055	Tangeretin	373	372	C20H20O7	[M + H]+	3403	2903	3227	3273	2773	2443	2963	2700	2850
52.Lmnp002584	5,7,4′-Trihydroxy-6-methoxyflavone-8-C-[β-D-glucosyl-(1–2)]-β-D-glucoside	625	624	C28H32O16	[M + H]+	9	9	66700	9	9	152000	9	23533	153000
53.Lmnp002448	5,7,3′,4′-Tetrahydroxy-6-methoxyflavone-8-C-[β-D-glucosyl-(1–2)]-β-D-glucoside	641	640	C28H32O17	[M + H]+	9	9	188667	9	9	297333	9	9	299000
54.Hmmp002121	Isorhamnetin-*O*-gallate	469	468	C23H16O11	[M + H]+	8936	82400	26533	949	110933	2083	619	13513	9
55.Hmcp001859	Isorhamnetin-*O*-rutinoside	625	624	C28H32O16	[M + H]+	9	1773	67033	9	9	164333	9	24867	173667
56.GQ512005	Kaempferol-3-*O*-glucoside-7-*O*-rhamnoside	595	594	C27H30O15	[M + H]+	9	12533	869	9	4627	653	9	159333	1300
57.pme0369	Kaempferol 3-*O*-rutinoside (Nicotiflorin)	593	594	C27H30O15	[M−H]-	363	183667	7647	1780	64833	10727	1616	1860000	14920
58.Lmmp003217	Kaempferol 3-*O*-β-*d*-(6″-*O*-(E)-*p*-coumaroyl)glucopyranoside	595	594	C30H26O13	[M + H]+	1491	265000	15300	1293	77600	16333	2150	2850000	18867
59.Lmbp003230	Kaempferol-3-*O*-neohesperidoside	595	594	C27H30O15	[M + H]+	9	254000	10567	866	92233	12097	1733	3723333	14900
60.Lnrp002296	Kaempferol glc-rha	595	594	C27H30O15	[M + H]+	1950	626333	31233	3663	251333	38300	8850	6516667	30400
61.Lmbp002592	Kaempferol-3,7-di-*O*-β-D-glucopyranoside	611	610	C27H30O16	[M + H]+	9	9	34667	9	9	62067	9	40400	90900
62.CWJP002348	Kaempferol-3-*O*-rhamnosyl-sophoroside-7-*O*-glucoside	949	948	C43H48O24	[M + H]+	416	436	202000	332	1143	254333	9	9	434000
63.Lmbp003393	Quercetin-3-*O*-α-L-rhamnopyranoside	449	448	C21H20O11	[M + H]+	646	50033	4530	9	29333	5813	873	592667	2993
64.Lmmp002859	Quercetin glucoside-glucoside	627	626	C27H30O17	[M + H]+	2215	25410	13167	7437	8207	33833	1647	1283	52100

(*Continued on next page*)

Table 1. *Continued*

Metabolite Index	Compounds	Q1 (Da)	Molecular Weight (Da)	Formula	Ionization model	YS1[a]	RS1[a]	PS1[a]	YS2[a]	RS2[a]	PS2[a]	YS3[a]	RS3[a]	PS3[a]
65.Hmmp002336	Quercetin-*O*-feruloyl-Pentoside	611	610	C30H26O14	[M + H]+	899	28267	44700	3536	37667	58933	893	52800	57000
66.Hmmp002041	Quercetin-*O*-Hexoside-*O*-rhamnoside-*O*-rhamnoside-*O*-Hexoside	919	918	C39H50O25	[M + H]+	9	9	179333	9	9	273667	9	9	547003
67.Lmln001801	Myricetin-3,7-*O*-dirhamnoside	625	626	C27H30O17	[M−H]-	9	9	10110	9	9	23100	9	9	32700
68.pmp001310	6-Hydroxykaempferol-3,6-*O*-Diglucoside	627	626	C27H30O17	[M + H]+	9	23640	16400	5723	7706	35533	1419	860	77467
69.Hmmp002189	Isorhamnetin-*O*-Hexoside-*O*-rhamnoside-*O*-rhamnoside-*O*-Hexoside	933	932	C40H52O25	[M + H]+	3103	3856	2903333	9	15540	6090000	9	9606	8903333
70.Hmmp002008	Isorhamnetin-*O*-Hexoside-*O*-rhamnoside-*O*-Hexoside-*O*-Hexoside	949	948	C40H52O26	[M + H]+	9	9	268667	9	9	301000	9	9	416000
71.Hmmp002240	Isorhamnetin-*O*-Hexoside-*O*-rhamnoside-*O*-glucuronate-*O*-Hexoside	963	962	C40H50O27	[M + H]+	9	9	407333	9	9	592000	9	1499	559000
72.Lmhp002800	2′-Hydoxy,5-methoxy Genistein-4′,7-*O*-diglucoside	641	640	C28H32O17	[M + H]+	9	9	90067	9	9	247333	9	9	229333

Note: Y, R, and P represent potato clones CIP 302281.17, CIP 302281.25, and CIP 302281.15, respectively; S1, S2, and S3 represent tuberization, tuber bulking, and tuber maturation stages, respectively, as shown in Figure 1.

[a]Relative amounts of flavonoids in potato tubers at three stages. The number 9 represents this kind of flavonoid was not detected1–24 = Anthocyanins25 = Dihydrochalcone26–27 = Dihydroflavones28 = Dihydroflavonol29–32 = Flavan-3-ols33–53 = Flavones54–71 = Flavonols72 = Isoflavone

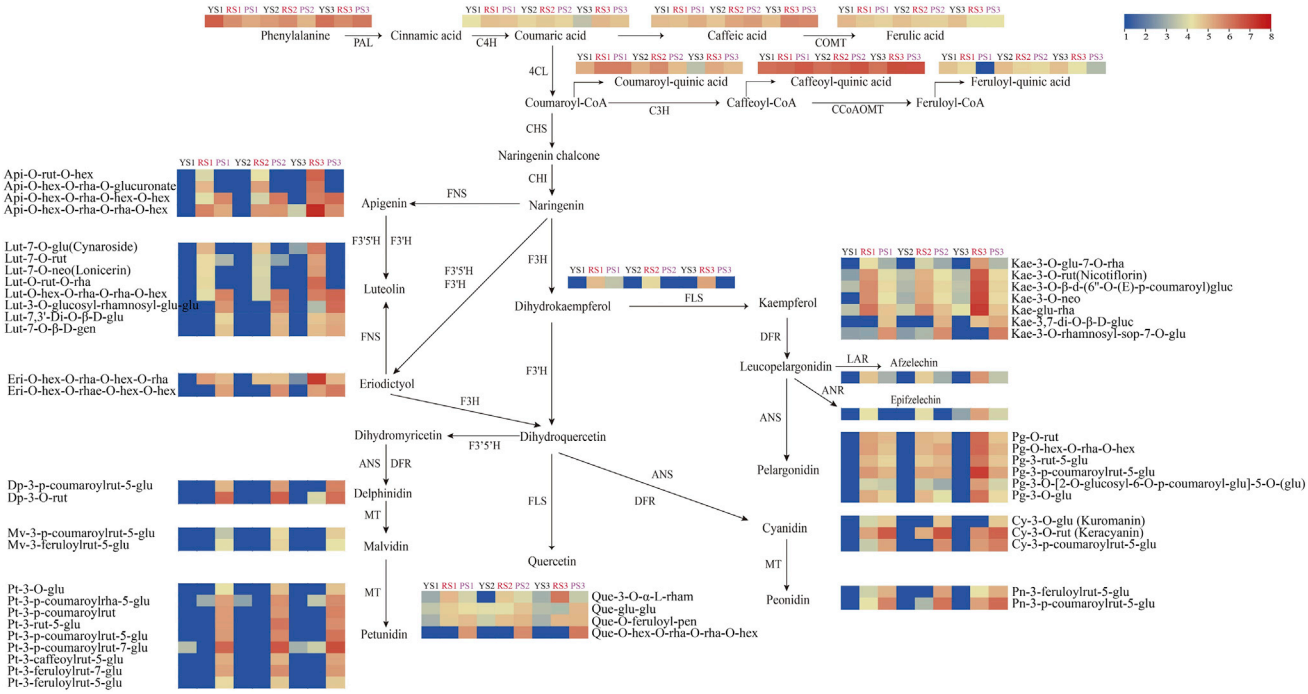

Figure 2. Heatmap of metabolites of flavonoid synthesis pathway in tuber flesh of three potato clones at three developmental stages

The pathway was built based on the KEGG pathway and references. Each colored cell represents the values of each compound ion normalized by converting into log10 unit according to the color scale (average value of three biological replicates × three clones × three stages, n = 9). Api, apigenin; Cy, cyanidin; Dp, delphinidin; Eri, eriodictyol; gen, gentiobioside; glu, glucoside; gluc, glucopyranoside; hex, hexoside; Kae, kaempferol; Lut, luteolin; Mv, malvidin; Nar, naringenin; *neo*, neohesperidoside; pen, pentoside; Pg, pelargonidin; Pn, peonidin; Que, quercetin; rha, rhamnoside; rham, rhamnopyranoside; rut, rutinoside; sop, sophoroside; PAL (phenylalanine ammonia-lyase); 4CL (4-coumarate-CoA ligase); C4H (*trans*-cinnamate 4-monooxygenase); CHI, chalcone isomerase; F3H, flavonoid 3-hydroxylase; F3′H, flavonoid 3′-hydroxylase; F3′5′H, flavonoid 3′5′-hydroxylase; DFR, dihydroflavonol 4-reductase; ANS, anthocyanidin synthase; FLS, flavonol synthase; FNS, flavone synthase; LAR, leucoanthocyanidin reductase; ANR, anthocyanin reductase. See also Table 1.

the P clone during tuber development; the high accumulation of Pg derivatives and with Cy and Pn derivatives in red flesh of R led to the red coloration at the S3 stage (Figure 2).

Transcriptome analysis of the tuber flesh of three potato clones at three stages

About 71.69%–88.58% of the clean reads were mapped to the reference genome. Out of 16,420 identified DEGs, between 548 and 4,706 were upregulated, while between 686 and 4,596 genes were downregulated (Figure S2). Differential Gene Ontology (GO) enrichment analysis focused on three major categories: molecular functions, cellular components, and biological processes, with p values <0.05. The carbohydrate derivative binding, anion binding, and ADP binding in the molecular function; thylakoid, plastid envelope, and chloroplast envelope in the cellular component; and response to stimuli, response to stress, and response to chemicals in the biological processes were the top three terms with the lowest p values in each category (Figure S3 and Table S3).

We used systems biology approach by employing weighted gene co-expression network analysis (WGCNA) to investigate the gene regulatory network of flavonoid synthesis in potato tubers.[44] This analysis resulted in 22 distinct modules (Table S4). The analysis of the modules revealed that three modules (grey60, greenyellow, and royalblue) were highly and positively correlated with most of the anthocyanins, flavonols, dihydroflavonols, flavones, dihydroflavones, flavan-3-ols, and dihydrochalcones, whereas two modules (green and red) had a high negative correlation (Figures 3A–3C). The results indicated that the genes within these modules may be involved in synthesizing flavonoids in tuber flesh during development.

The three gene sets (grey60 modules 118 genes, greenyellow 556 genes, and royalblue modules 63 genes) were positively correlated with flavonoids; of these, a significant correlation was particularly found between the grey60 module and flavonoid metabolites in the red flesh of R ($r^2 > 0.86$, $p < 1e\text{-}08$), such as all Pg

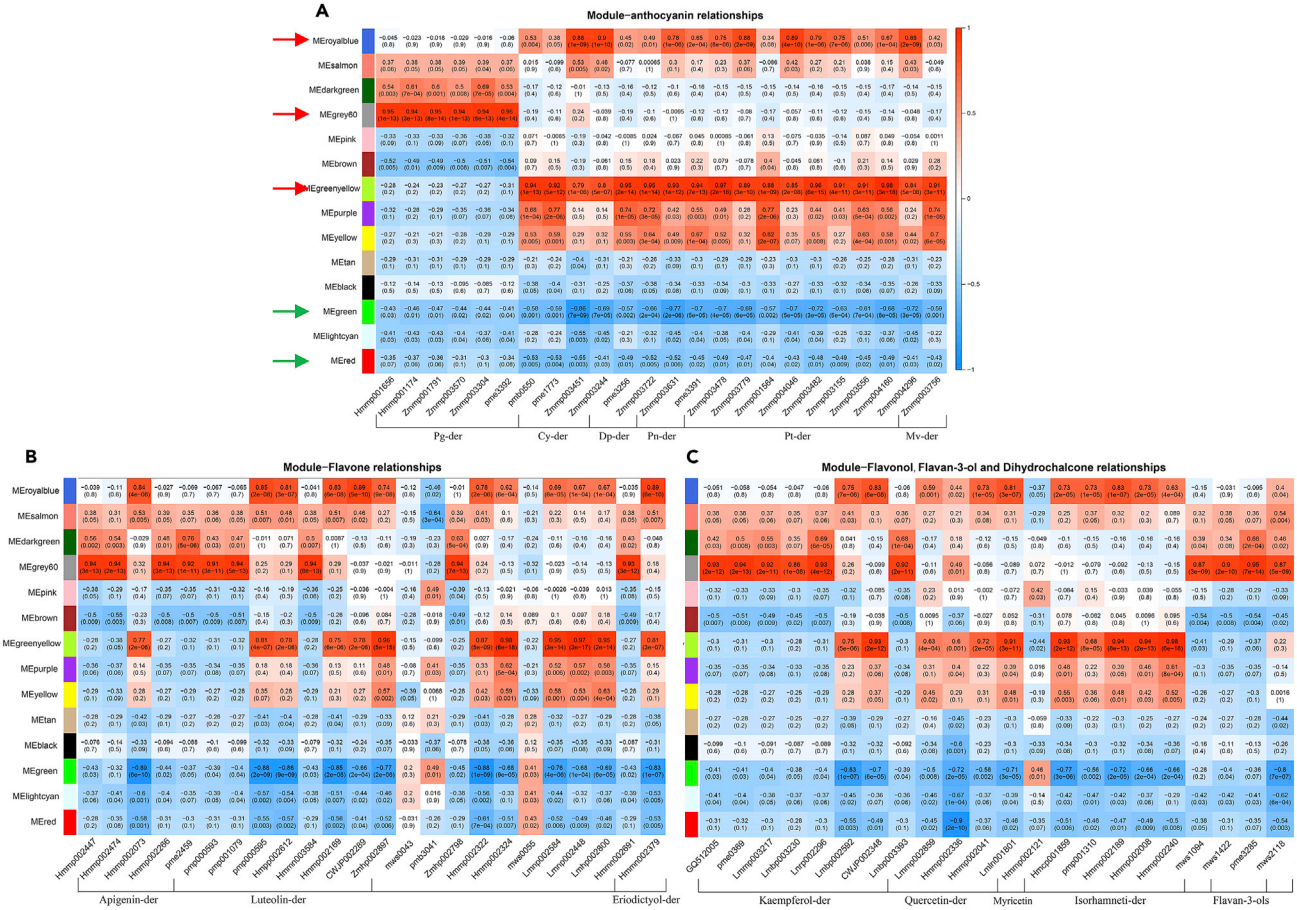

Figure 3. Weighted gene co-expression network analysis (WGCNA)

(A-C) Module–flavonoid relationship. A row and column respectively indicate a module and a specific flcvonoid compound in potato clones (details in Table 1). Each cell's value represents the correlation coefficient between a module and the flavonoid and is displayed based on the color scale on the right. p values are shown in parentheses in the center of each cell. The red or green arrows indicate the modules with higher positive or negative correlation with flavonoid compounds.

(A) module-anthocyanin relationships; (B) module-flavone relationships; (C) module-flavonol, flavan-3-ols, and dihydrochalcone relationships. See also Tables 1 and S4.

derivatives, apigenin, luteolin, and kaempferol derivatives (Figure 3). These genes were highly upregulated or downregulated in the red flesh of R according to kME (eigengene-based connectivity) value (Figure 4A), whereas the genes in greenyellow module were more closely related to the flavonoid metabolites in the purple flesh of P (Figure S4A). Enrichment analysis of GO terms revealed that for genes co-expressed in the grey60 module, "response to UV-B" as well as the biosynthesis of "flavonoid" and "phenylpropanoid" was significantly enriched biological processes (Figure 4B and Table S5). In contrast, the "DNA recombination", "organelle organization", and "mitochondrial transmembrane transport" biological processes were significantly enriched in the greenyellow module, while in the royalblue module, significantly enriched genes were mostly involved in "heterocycle metabolism", "regulation of developmental process", and "organic cyclic compound metabolism" (Figures S4A and S4B, Table S5).

Gene networks were further constructed and visualized by WGCNA and Cytoscape for identifying key hub regulatory genes within these modules.[45] In this case, an edge weight ≥0.15 was selected, with each node and the connecting lines (edges) representing a gene and co-expression relationships, respectively. For the analysis, it was assumed that key regulatory genes were more likely to be found in hub genes having most connections within the network.

In the grey60 module network, most genes were flavonoid-related pathway genes, while *StCHI* (Soltu. DM.05G022280) was the hub gene having most edges (26), followed by *StPAL* (Soltu. DM.05G026870)

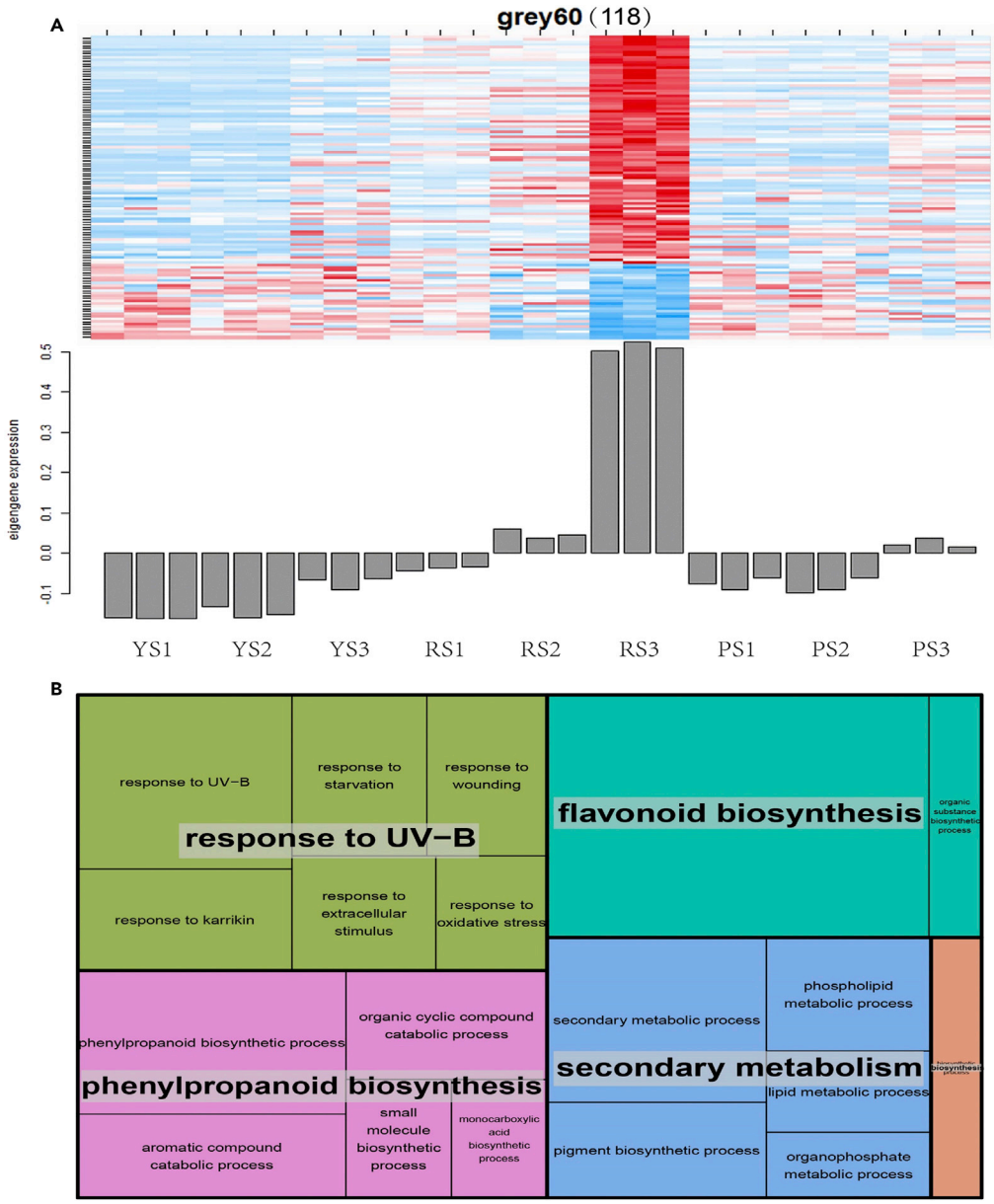

Figure 4. Expression profiles, functions of genes in grey60 module, which is positively correlated with flavonoid compounds

(A) Eigengene expression values and heatmap based on FPKM of each gene of grey60 module. The eigengene value of the module or gene is shown on the y axis; the x axis indicates the type of potato clones (Y, R, and P) and the three developmental stages (S1, S2, and S3). The number of genes in grey60 module is indicated at the top.

(B) Results of the analysis of enriched GO terms for the grey60 module as visualized by the "TreeMap" view of REVIGO. Common colors represent groupings based on parent GO terms, and each rectangle is a single cluster representative for the non-redundant GO term. The representatives are joined into "superclusters" of loosely related terms, visualized with different colors. The size of the rectangles reflect the p value. See also Tables S4 and S5.

with 23 edges. In green-yellow module network, Soltu. DM.10G014550, of unknown function, had most edges (113), followed by a DNA repair protein (Soltu. DM.07G017450) with 103 edges. In royalblue module network, histone deacetylase *HDT2-like* gene Soltu. DM.04G014010 and *myosin-11-like* gene Soltu.DM.06G001190 are the hub genes with the highest number of edges (9 edges and 8 edges, respectively) (Table S6).

The green module (1237 genes) was strongly negatively correlated with most of the flavonoids, and the red module was also negatively correlated with most flavonoids (Figure 3). The StAN1 (Soltu. DM.10G020850)—anthocyanin biosynthesis activator of the potato tuber—and the cofactor StbHLH1 (Soltu. DM.09G019660)[18] were assigned into the red and green modules, with kME value −0.8 and −0.9 (Table S4). The *F3′5′H* (Soltu. DM.11G020990) and *DFR* (Soltu.DM.02G024900) genes within the anthocyanin biosynthesis pathway were assigned into the green module, with kME value −0.9, showing they were highly upregulated in the colored flesh of R and P (Table S4). The anthocyanin cofactor StbHLH1 was also in the green module with a strong negative correlation, suggesting the expression of *F3′5′H* and *DFR* pathway genes was more likely to be associated with *StbHLH1*, which was only highly upregulated in colored flesh. The expression level was consistent with an anthocyanin accumulation trend.

In the red module network, high expression of genes with positive kME values was only observed for white and yellow tuber flesh of Y, whereas the genes with negative kME values were highly upregulated in the flesh of R and P at three stages. "DNA recombination" and "ribosome biogenesis" represented the main biological processes in which these genes were mainly involved (Figure S4). The anthocyanin activator StAN1 was assigned to the red module with a significantly negative correlation (kME = − 0.8) (Table S4). Unlike *F3′5′H*, *DFR* and *StbHLH1* expression levels, *StAN1* was highly upregulated in the flesh of R and P at three stages (Table S4), suggesting *StAN1* was activated at the initial developmental stage of the tuber in colored cultivars, to participate in regulating flavonoid biosynthesis.

Expression of flavonoid synthesis-related genes in three potato clones

We identified 8 differentially expressed *PALs*: 2 of them (Soltu. DM.09G005690 and Soltu. DM.05G026870), named *PAL-1* and *PAL-2*, were in module grey60, which were highly expressed in colored flesh, suggesting the two *PALs* were involved in flavonoid biosynthesis (Figure 5). Five *4CLs* and 3 *C4Hs* were identified in our dataset; the relatively high expression of *4CL-4*, *C4H-2*, and *C4H-3* in tuber flesh ensured the production of precursor compounds for the phenolic and flavonoid biosynthesis. CHS and CHI are key enzymes controlling flavonoid biosynthesis. In the present study, we identified two *CHSs* and two *CHIs*, belonging to module grey60, which were highly expressed in tuber flesh of R and P at three developmental stages, and the highest expression level was present in red flesh of R at S3. In RS3, a consistently high expression of *F3H* results in the production of dihydrokaempferol. DFR and FLS use dihydrokaempferol, dihydroquercetin, or dihydromyricetin as the substrate for respectively producing colored anthocyanins and colorless flavonols such as kaempferol, quercetin, or myricetin, with the level of *FLS* and *DFR* expression influencing the amount of both compounds.[46] The kaempferol, quercetin, and myricetin derivatives in RS3 and PS3 were highly accumulated in our datasets (Figure 2 and Table 1); however, the *FLS* transcription levels identified did not correlate with flavonol content. The high expression of *UFGT*, *ANS*, and *DFR* in RS3 led to a high accumulation of Pg derivatives. In addition, the *F3′5′H* also showed high expression in RS3, leading to the production of Cy derivatives, thus the flesh red color. We also found the monomeric precursors—flavan 3-ols (in this case afzelechin and epifzelechin)—were highly accumulated in RS3, which were formed via the reduction of leucopelargonidin by LAR or via the reduction of pelargonidin by ANR.[47] 2 *ANR* genes were identified, but no *LAR* was detected in our work, suggesting the other genes were involved.

In purple flesh, the *F3′H* was weakly expressed, but high luteolin, eriodictyol, myricetin, quercetin, Dp, Pt, Mv, and Pt derivatives contents were accumulated, suggesting the highly expressed *F3H* and *F3′5′H* genes, coupled with the high expression of *UFGT*, *ANS*, *DFR*, and *AOMT*, were mainly responsible for affecting flavonoid biosynthesis by routing flux through dihydromyricetin, dihydroquercetin, and luteolin. This led to the increased accumulation of Dp, Pt, Mv, and Pt derivatives, finally resulting in the dark-purple color in tuber flesh of P at stage S3. GSTs, MATEs, and the ABC proteins act as carrier proteins for sequestering anthocyanin and proanthocyanidin (PA) within vacuoles.[7] We found two *GSTs*, one *MATE*, and two *ABC transporters* in module grey60 which could very likely participate in flavonoid synthesis. Also, a plasma membrane H + -ATPase energizes TT12—the MATE transporter for the import of PAs into the vacuole.[48] In our dataset, we identified an *F-type H+-ATPase* (Soltu. DM. 02G026440) in the grey60 module highly expressed in tuber flesh of R at stage three, which could be responsible for this function (Figure 5).

Flavonoid synthesis regulated by transcription factors

In the grey60 module, one *R2R3-MYB* (Soltu.DM.05G004700) and one *MYB-related* (Soltu.DM.12G023200) TF showed high intra-modular connectivity with kME value > 0.9, highly expressed in colored flesh. In the

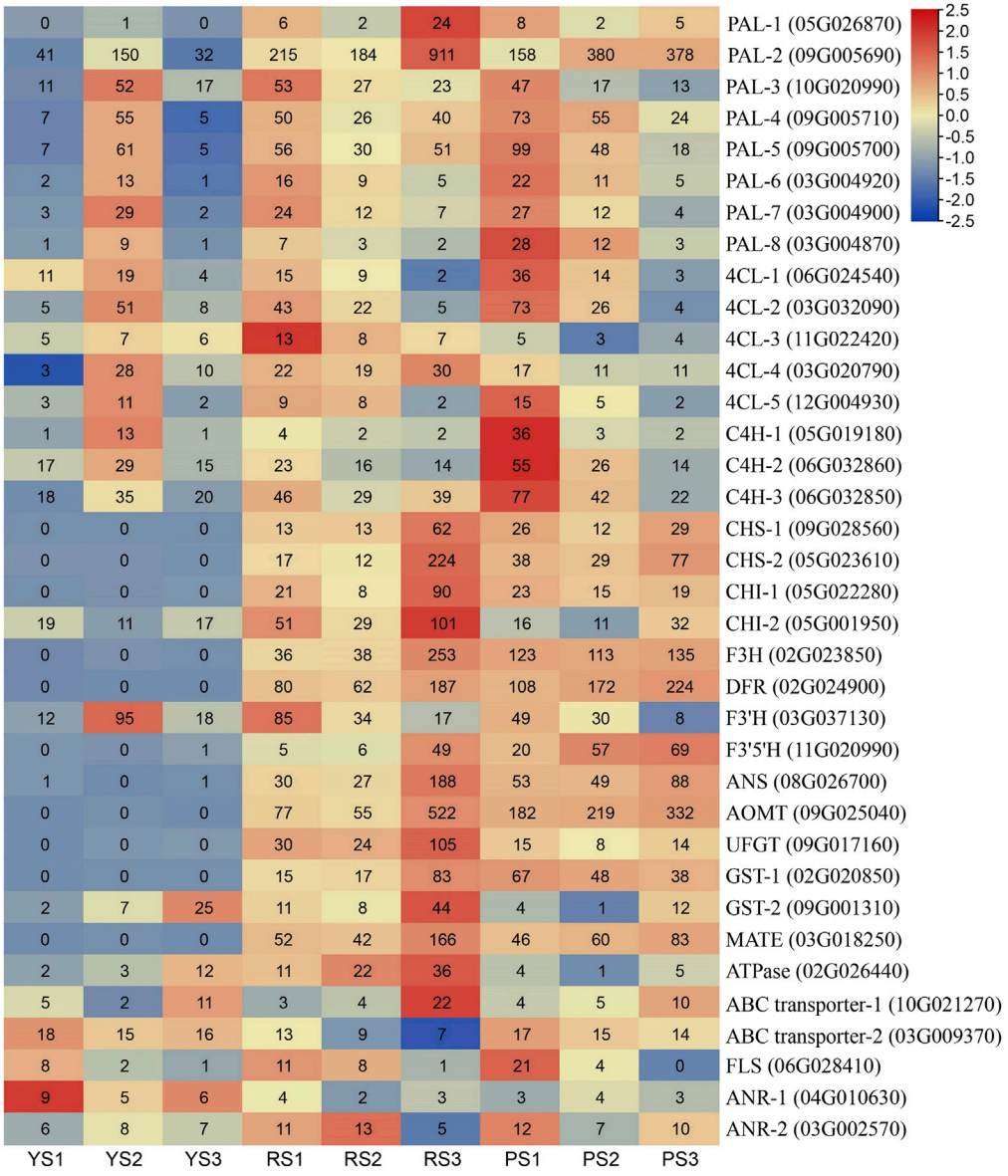

Figure 5. The expression profile of major flavonoid-related genes in tuber flesh of Y, R, and P potato clones at three developmental stages

Each row and column represent a gene and a library, respectively. The blue to red color of cells represent the log2-transformed FPKMs normalized by row scale. The original FPKM values are shown in the middle of each cell. Gene IDs were presented in parentheses and "Soltu.DM." was omitted for clarity. *PAL (phenylalanine ammonia-lyase); 4CL (4-coumarate-CoA ligase); C4H (*trans*-cinnamate 4-monooxygenase); CHS (chalcone synthase); CHI (chalcone isomerase); F3H (naringenin 3-dioxygenase); DFR (dihydroflavonol 4-reductase); F3′H (flavonoid 3′-monooxygenase); F3′5′H (flavonoid 3′, 5′-hydroxylase); AOMT (flavonoid 3′,5′-methyltransferase); ANS (anthocyanidin synthase); UFGT (UDP-glucose flavonoid 3-O glucosyltransferase); GST (glutathione transferase); MATE (Multidrug and toxic extrusion); ABC transporter (ATP-binding cassette transporter); FLS (flavonol synthase); ANR (anthocyanidin reductase).

greenyellow module, 22 genes were identified as TFs or transcriptional regulators (TRs), and six of them showed higher absolute values of kME (>-0.8), including zinc finger TFs (*C2C2* and *C3H*), *STK*, *SNF2*, and *ARID* families. In the green module, 36 genes were assigned as TFs or TRs, and 12 of them showed high absolute values of kME (>0.8), of which two *C2C2-GATA* TFs and three *SET* TRs were in the positive kME sets. They were all downregulated in colored flesh, whereas seven TFs, including *bHLH1*, *C2H2*, *BPC*, *MYB-related*, *HB* TFs, and *PHD*, *GNAT* TRs, were all upregulated in colored flesh. In the red module, 14

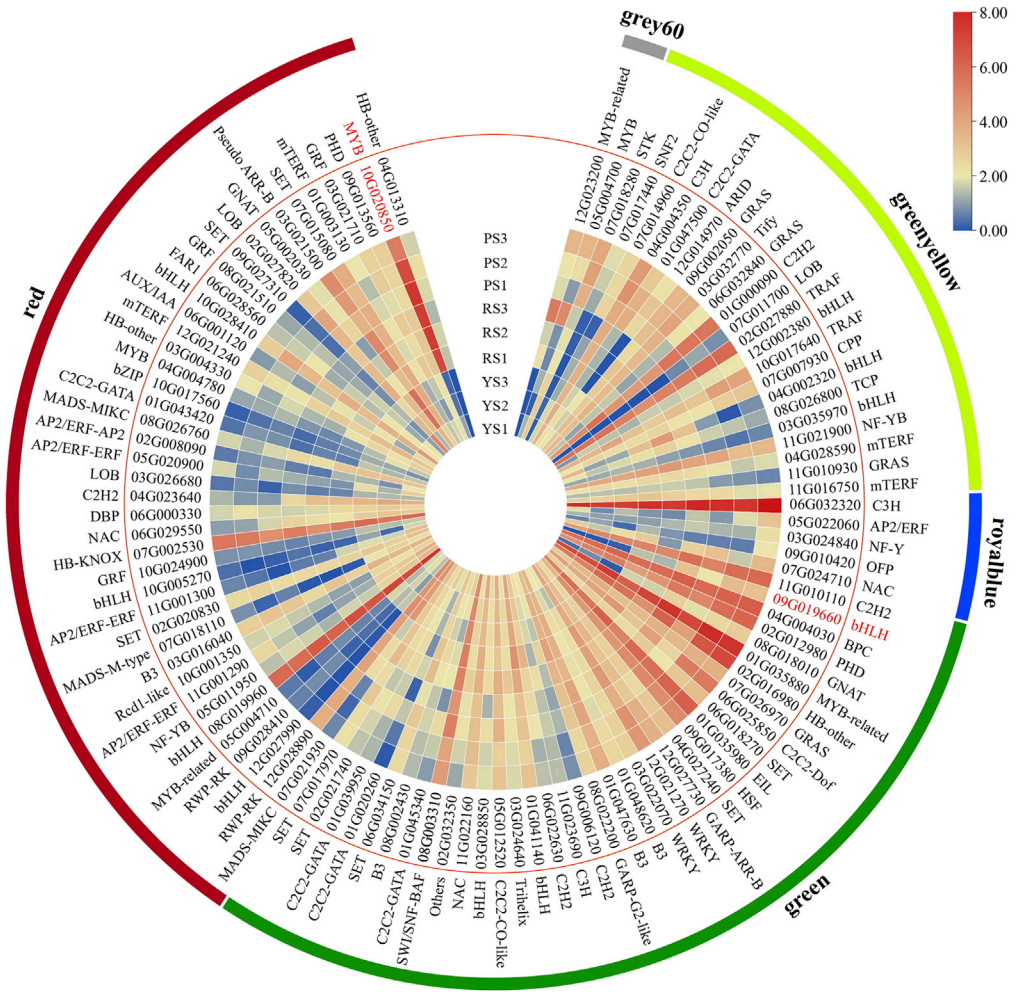

Figure 6. The expression profile of transcription factors in tuber flesh of Y, R, and P potato clones at three developmental stages in grey60, greenyellow, royalblue, green, and red modules

The blue to red color of cells represent the log2-transformed FPKMs. "Soltu.DM." in Gene ID was omitted for clarity. The TFs StAN1 (Soltu.DM.10G020850) in red module and StbHLH1 (Soltu.DM.09G019660) in green module were shown in red color. See also Table S4.

out of 42 TFs or TRs showed a high absolute value of kME (>0.8). In the positive kME sets, TFs upregulated in white or yellow flesh of Y included a *bHLH* showing high expression with the Fragments Per Kilobase of transcript per Million fragments mapped (FPKM) >100; one *MADS-MIKC* (AtAGL1-like) and one *RWP-RK* were highly expressed with an FPKM >20 (Figure 6). The anthocyanin activator *StAN1* was highly expressed in tuber flesh of R and P at three stages. The *HB-other* TF (Soltu.DM.04G013310) displayed an overlapping expression pattern with StAN1, but the FPKM was relatively low (between 1 and 4) (Figure 6). Thus, apart from the reported anthocyanin-related *StAN1* and *StbHLH1* TFs, other TFs in the same module displayed similar expression patterns to those of *StAN1* and *StbHLH1*, thereby suggesting their potential involvement in regulating the synthesis of flavonoids in potato tuber flesh.

MYBs identified that repress anthocyanin biosynthesis

The grey60 module was the main one associated with the flavonoid compounds (highest positive correlation; Figure 3). Within this module, co-expressed genes were significantly enriched for "flavonoid biosynthesis" (Figure 4B), and most of the flavonoid-related genes were classified into the module grey60 (Figure 5 and Table S4). Thus, the genes in grey60 module were further analyzed, with results indicating that 34 genes were correlated with an edge weight ≥0.15 (Table S6). Only two TFs—an R2R3-MYB TF (Soltu.DM.05G004700) and an MYB-related (Soltu.DM.12G023200) TF—were included in this network,

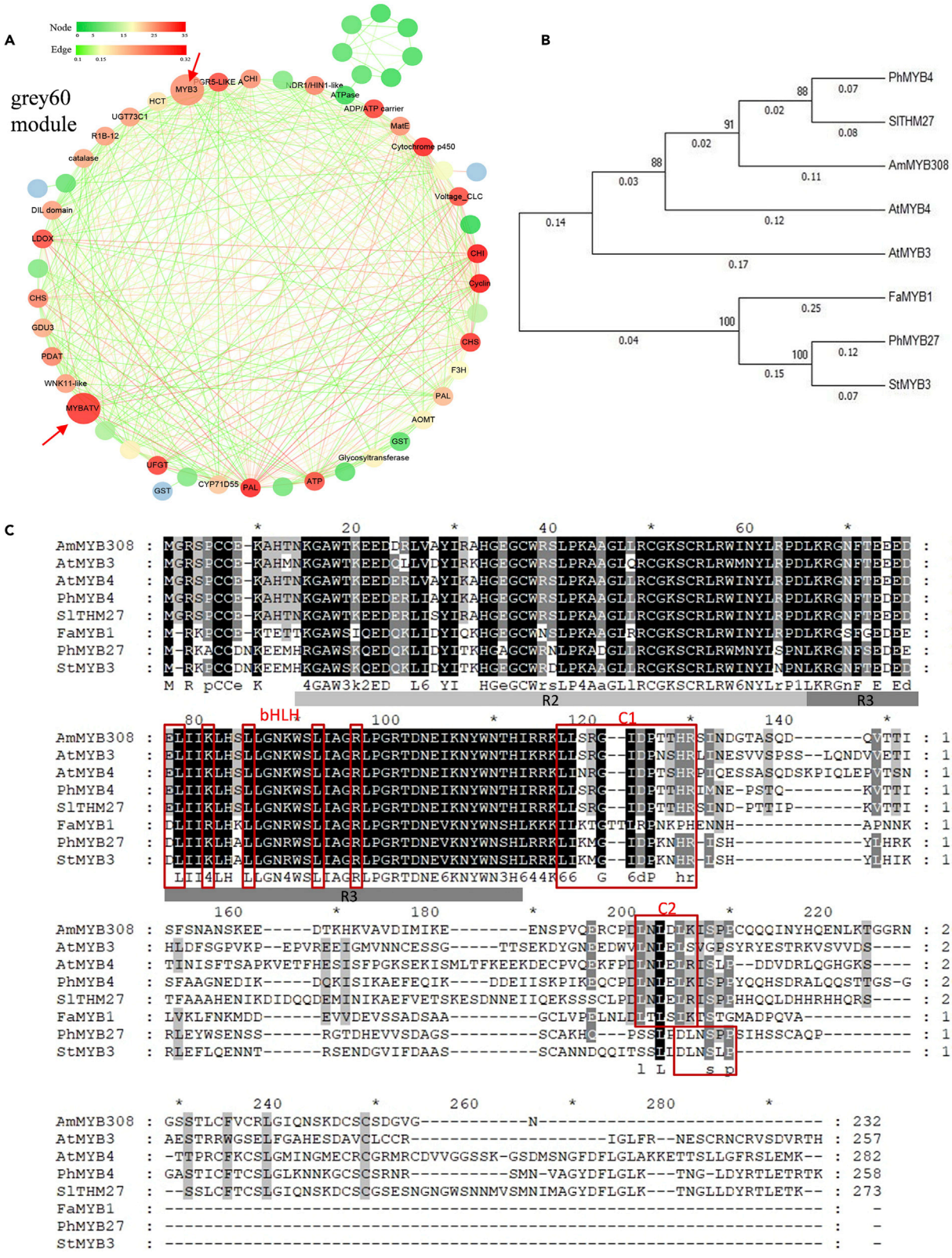
A
Node
Edge
grey60
module
MYB3
MYBATV
HCT
UGT73C1
R1B-12
catalase
DIL domain
LDOX
CHS
GDU3
PDAT
WNK11-like
UFGT
GST
CYP71D55
PAL
ATP
Glycosyltransferase
AOMT
GST
PAL
CHS
F3H
CHI
Cyclin
Voltage_CLC
Cytochrome p450
MatE
ADP/ATP carrier
ATPase
DR1/HIN1-like
CHI
B
PhMYB4
SlTHM27
AmMYB308
AtMYB4
AtMYB3
FaMYB1
PhMYB27
StMYB3
C
bHLH
R2
R3
C1
C2

Figure 7. Network of correlated genes within the grey60 module and the sequence analysis of StMYB3

(A) Network was visualized by Cytoscape. The hub TFs StMYB3 and StMYBATV are shown by large circles with red arrows. The green to red color of nodes represents the degree of connectivity, the green to red color of edges represents the weight above a threshold of 0.1.

(B and C) Phylogenetic tree and amino acid sequence alignment of StMYB3, AtMYB3, AtMYB4, PhMYB27, FaMYB1, AmMYB308, SlTHM27, and PhMYB4; the StMYB3 shares high identity with PhMYB27 and FaMYB1. A black color indicates conserved and partially conserved residues while grey and greyish white boxes respectively show the R2 and R3 domains. The red boxes show the conserved motifs C1 and C2 in the C-terminus. The following GenBank accession numbers are used: AmMYB308 (P81393.1), AtMYB3 (NP 564176.2), AtMYB4 (NP 195574.1), PhMYB4 (F1B281.1), SlTHM27 (NP_001233975.1), FaMYB1 (AAK84064.1), PhMYB27 (AHX24372.1), and StMYB3 (MW768000). See also Table S6.

with kMEs of 0.92 and 0.91, respectively, and a high degree of connectivity suggesting they are the hub genes in this module (Figure 7A). Based on phylogenetic analysis, Soltu.DM.05G004700 clustered with AtMYB3 and AtMYB4, which belong to group 4 of the MYB proteins in *Arabidopsis*[49]; therefore it was annotated as StMYB3. The deduced protein of Soltu. DM.05G004700 shares high identity with PhMYB27, FaMYB1, and AtMYB3. Two conserved domains in the C terminus of the subgroup 4 type MYB TFs, C1(LlsrGIDPx $T/_N$ HR) and C2/EAR motif (LxLxL or DLNxxP), which are required for their repressive activity, were found in StMYB3 (Figures 7B and 7C). By BLAST analysis of Soltu.DM.12G023200, it was completely identical with the reported StMYBATV, which was characterized as an anthocyanin negative regulator in potato cell culture,[42,50] and therefore Soltu.DM.12G023200 was annotated as StMYBATV.

The CDS of *StMYB3* was cloned and transformed into *Nicotiana tabacum* by transient *Agrobacterium* infiltration assays. Based on transient color assays, it was found that anthocyanin production was not induced in tobacco leaves after infiltration of StMYB3 alone, but an intense red pigmentation was observed following infiltration with StAN1-R1 as an anthocyanin activator.[18] On the other hand, co-infiltration of StAN1-R1 with StMYB3 resulted in the absence of pigmentation after 4 days (Figure 8A). After 7 days, accumulated anthocyanin with dark red coloration was observed in the leaf infiltrated with StAN1-R1, while very light red was seen in leaf tissue infiltrated with combined StAN1-R1 and StMYB3 (Figure 8A). These results indicate that StMYB3 was able to suppress anthocyanin accumulation. To further verify the suppressive ability of StMYB3 to block anthocyanin biosynthesis, StMYB3 was infiltrated into the young leaves of transgenic tobacco that constitutively overexpresses the anthocyanin activator *StAN1-R1*. The results showed that anthocyanin accumulation was repressed in transgenic tobacco leaves that transiently overexpressed *StMYB3* (Figure 8B).

Using cDNA of tuber flesh of R at the S3 stage, the CDS of *StMYBATV* was cloned. Based on phylogenetic analysis, it was found that StMYBATV belongs to the R3-MYB group, which included TRICHOMELESS (TLC1), ENHANCER OF TRY AND CPC (ETC), TRIPTYCHON (TRY), AtMYBL2, and CAPRICE (CPC) that negatively influence anthocyanin synthesis.[51] To further confirm the repressive function of StMYBATV, it was transformed into *N. tabacum* by transient assays as well. The transient color assays in tobacco leaves showed accumulated anthocyanin, with dark red observed in the leaf infiltrated with StAN1-R1, while light red was seen in leaf tissue infiltrated with combined StAN1-R1 and StMYBATV after 7 days of infiltration (Figure 8C).

To assess how StMYB3 and StMYBATV influenced gene expression in the anthocyanin pathway, *prom-3-StDFR*, a promoter of the DFR gene in potato, was fused with the luciferase reporter.[18] Co-infiltration of StAN1-R1 with StbHLH1 activated the promoter, while co-infiltration of StMYB3 or StMYBATV inhibited the gene activity. The repressive function of either StMYB3 or StMYBATV alone or a combination of StMYB3 and StMYBATV showed no significant difference (Figure 8D). These results further confirmed that StMYB3 and StMYBATV negatively regulate the synthesis of anthocyanins.

It was previously reported that in potato tubers, StAN1 acts together with StbHLH1 for regulating anthocyanin biosynthesis.[18] The bHLH binding domain was also found in StMYB3 and StMYBATV. To further investigate whether StMYB3 and StMYBATV interacted with StbHLH1, the StMYB3/StMYBATV and StbHLH1 recombination vectors were constructed and used for yeast two-hybrid and BiFC assays. The results showed that on selective medium, only cells expressing both MYB repressors and the StbHLH1 factor showed growth (Figure 8E). Via *Agrobacterium*-mediated transformation of *Nicotiana benthamiana* leaves, the epidermal cells of StMYB3-StbHLH1 and StMYBATV-StbHLH1 combinations in *N. benthamiana* displayed fluorescence signals (Figure 8F).The result suggests that both repressors StMYB3 and StMYBATV can inhibit the synthesis of anthocyanin by interacting with StbHLH1 to compete with anthocyanin activator StAN1during tuber development (Figure 9).

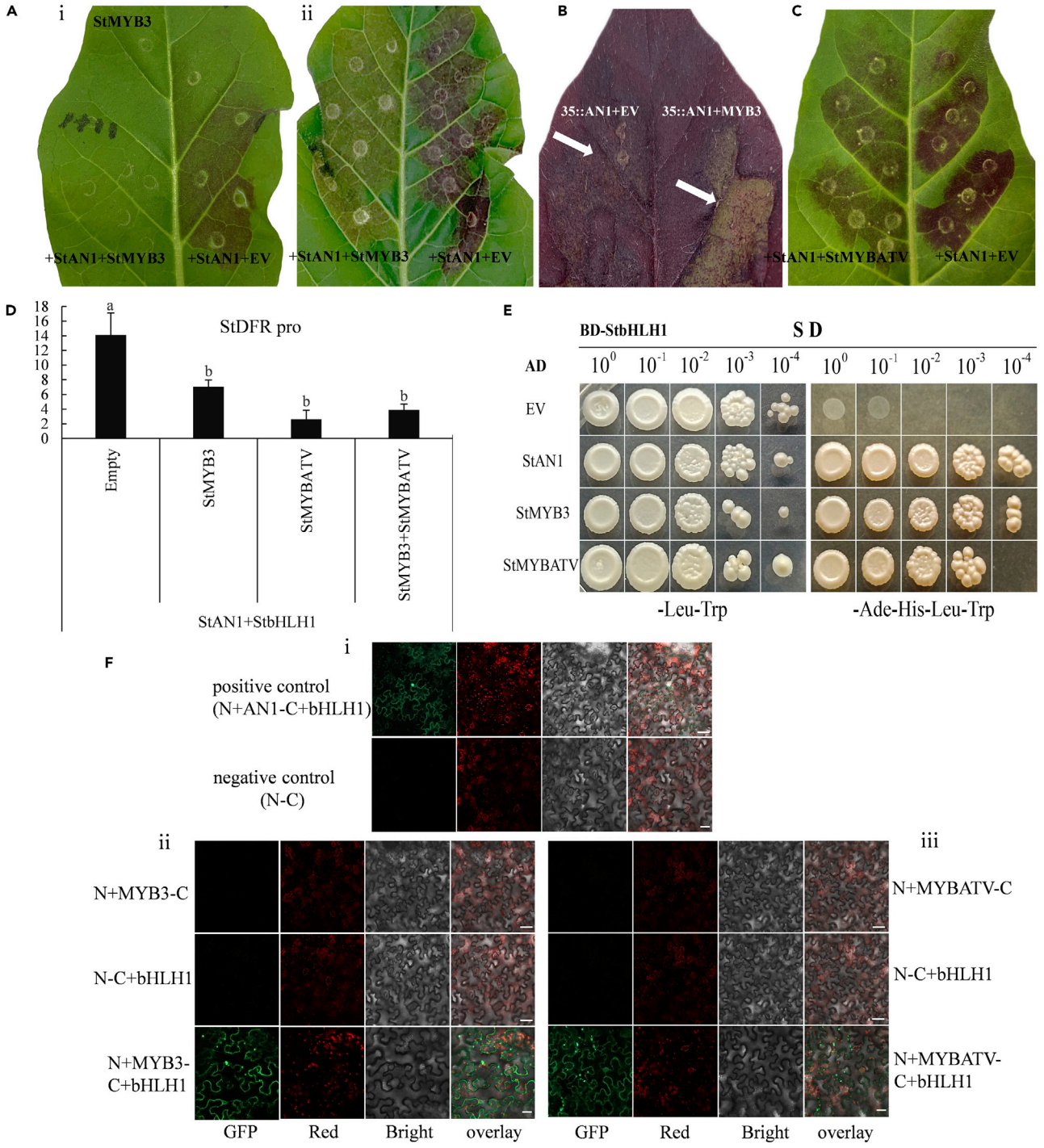

Figure 8. Functional analysis of the potato StMYB3 and StMYBATV TFs

(A) Infiltration with StMYB3 only, a combination of StAN1-R1 and StMYB3 or a combination of StAN1-R1 with an empty vector (EV) was carried out on the upper left side, on the lower left side and on the right side of a tobacco leaf respectively; Pictures were taken four days (i) and seven days after infiltration (ii).

(B) Transgenic tobacco constitutively overexpressing *StAN1-R1* was used to transiently overexpress *StMYB3* (right side of the tobacco leaf) and EV was used as control (left side of the tobacco leaf), the infiltrated tissues were indicated by white arrow.

(C) Co-infiltration of StAN1-R1 and StMYB3 (left side of tobacco leaf) and StAN1-R1 (right side of the tobacco leaf).

(D) StMYBATV and StMYB3 prevent the activation of the promoter StDFR-LUC, by co-filtration with StAN-R1 and StbHLH1 using dual luciferase assay. Error bars (SE) are provided for four biological replicates. Data are represented as mean ± SE. One-way ANOVA was used to determine the statistical significance

Figure 8. *Continued*

of results, with means compared by Least Significant Difference (LSD) to identify significant differences at $p < 0.05$. Different letters (a, b, c, etc.) above the bar indicate significantly different means.

(E) StbHLH interacts with StMYB3 and StMYBATV in yeast. Yeast cells were grown on -2SD (-Leu-Trp) or -4SD (-Ade-His-Leu-Trp) medium.

(F) Bimolecular fluorescence complementation assays show the interactions between StMYB3/StMYBATV and StbHLH1 proteins in epidermal cells of *N. benthamiana*, respectively. (i) Positive and negative controls. (ii) The interaction between StMYB3 and StbHLH1 proteins. (iii) The interaction between StMYBATV and StbHLH1 proteins. Scale bars, 20 μM.

qRT-PCR and RNA-seq datasets correlations

The RNA sequencing (RNA-seq) expression profile was validated by qPCR using gene-specific primers of eight differentially expressed structural genes and TFs. The results showed that despite variations between RNA-seq data and qPCR results in terms of relative expression of selected genes, linear regression analysis ($y = 0.9782x - 0.3605$) suggested a high correlation ($R^2 = 0.8838$), thus highlighting that the two analytical methods were consistent (Figure S5).

DISCUSSION

Anthocyanins are responsible for the red to purple pigmentation of potatoes, which is attractive to consumers. They not only confer resistance against biotic and abiotic stresses but also offer potential health benefits to humans, with some examples being intervention in several chronic diseases and protection against cardiovascular diseases as well as some cancers.[1,52] As a result, flavonoid production in colored potatoes has attracted increased interest, especially for understanding the underlying regulatory mechanism. The regulatory network involved in sprout pigmentation from three colored potato cultivars has been investigated based on integrated analysis of transcriptome and metabolome, and 119 genes that strongly correlated with 22 anthocyanins in sprouts were identified.[39] In our current study, metabolomic and transcriptomic differences among potato tubers of three different colored potato clones at three developmental stages were comprehensively analzyed, seeking to identify candidate genes that may be involved in flavonoid biosynthesis in potato tuber during tuber development phases.

Based on WGCNA analysis, three modules (grey60, greenyellow, and royalblue) were identified to be positively correlated with flavonoid biosynthesis and further analyzed, whereas several other modules were found to have a negative correlation with flavonoid biosynthesis. There were 118 genes in grey60, which showed a higher correlation ($r^2 > 0.9$) with Pg derivatives in the anthocyanin class; apigenin, luteolin, eriodictyol derivatives, and isosaponarin in the flavone class; and dihydrokaempferol, kaempferol, Quercetin-3-*O*-α-L-rhamnopyranoside, (−)-epiafzelechin, afzelechin, and phloretin 2′-*O*-glucoside in the flavonol and flavan-3-ol classes. In grey60, we found 13 kinds of biosynthetic pathway genes, such as two *PALs*, two *CHSs*, two *CHIs*, one *F3H*, one *ANS*, one *AOMT*, one *UFGT*, two *GSTs*, and one *MATE*. One *ATPase* and two *ABC transporters* had the highest expression levels in the red flesh of R, as well as increased expression levels in purple flesh of P at three stages, suggesting they are more likely to be responsible for the red pigmentation (Pg derivatives) and other flavonoid compound biosynthesis mentioned above. The identified *FLS* and *ANR* showed very low expression in the red flesh of R, at the S3 stage (FPKM 1 and 3–5, respectively), suggesting other candidate genes were involved because high accumulations of kaempferol, (−)-epiafzelechin, and afzelechin were detected in red flesh (Figure 2 and Table 1).

The transcriptional control of genes within the anthocyanin pathway by the MBW complex as well as the latter's influence on anthocyanin production and distribution has been widely studied.[12,53] The MBW complex is encoded by the TFs StAN1, StbHLH1, and StWD40 in potato tubers and leaves.[17,18,41,54]

StAN1 is the key regulatory gene regulating anthocyanin production in potatoes. However, diagnostic markers generated for functioning StAN1 alleles (StAN1-777 and StAN1-816) cannot be used to predict potato pigmentation variations successfully. The StAN1 promoter sequence organization is likely critical for anthocyanin synthesis control, necessitating the creation of additional diagnostic markers.[55] Increased expression of *StAN1-like* and *PAL* was associated with deeper colors of the potato, with *StAN1-like* being predominantly expressed in potato tubers, stems, and roots; its expression was however dramatically enhanced in Purple Meigui 2 and Red Meigui 3 potato tubers.[56,57] The anthocyanin activator *StAN1* was assigned to the red module with a negative relationship (kME > - 0.8). Interestingly, high expression of *StAN1* was observed in white/yellow flesh and colored flesh of R and P at three stages. The

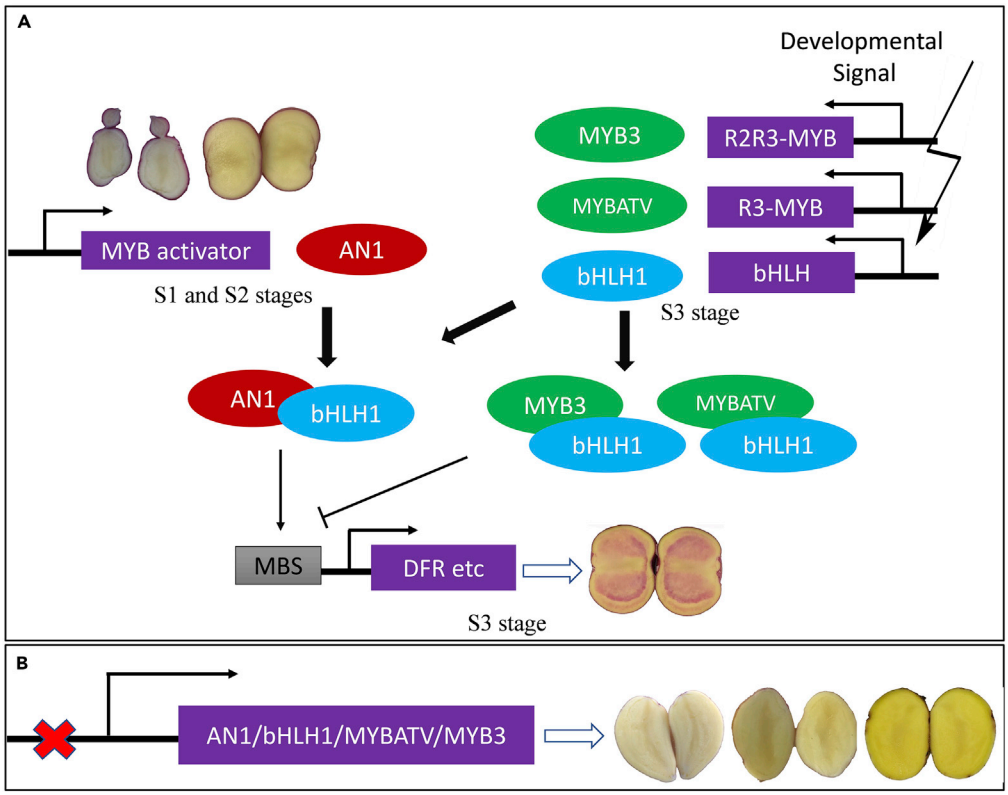

Figure 9. Schematic diagram of the anthocyanin regulation network in potato tuber flesh

(A) In red clone R, the R2R3-MYB activator—StAN1—was activated at S1 stage, the bHLH1 was activated at S3 stage and combined with StAN1 to activate the expression of the anthocyanin biosynthesis genes. Feedback inhibition is provided by an R2R3-MYB repressor StMYB3 and an R3-MYB repressor StMYBATV, which were also activated at S3 stage and inhibit gene expression (such as DFR) by combining with bHLH1 to prevent the synthesis of anthocyanins. MBS indicates MYB-binding sites.

(B) In yellow clone Y, TFs StAN1, StbHLH1, StMYB3, and StMYBATV were not activated at three stages.

anthocyanin pathway genes *F3′5′H*, *DFR*, and TF *StbHLH1* were classified into the green module with a negative elationship (absolute kME >0.88); they were highly expressed in all colored flesh and present in the highest expression in purple flesh of P at S3, which, combined with their relationship with anthocyanin metabolite analysis, suggest the two pathway genes and StbHLH1 may be crucial for regulating late biosynthetic genes (LBGs) to affect anthocyanin biosynthesis, by regulating the flux through purple-blue delphinidin.

Soltu.DM.10G025870, annotated as serine/threonine-protein kinase *SRPK3* by the Kyoto Encyclopedia of Genes and Genomes (KEGG) database, showed a high correlation with *StAN1* in this module (with edge weight $\geq$0.15). It has been reported that, as a plant-specific serine/threonine protein kinase, the sucrose non-fermenting 1-related kinase (SnRK) is involved in abscisic acid (ABA)-dependent and ABA-independent signaling pathways that regulate plant adaptation to abiotic stress[58]; the relationship between ABA and flavonoid biosynthesis in potato tuber is worthy of further investigation.

The MBW complex is reported to be sensitive to feedback repression by MYB repressors.[59] FaMYB1, the first anthocyanin-related R2R3-MYB repressor was identified in strawberry. Although it is highly expressed during the red ripening stages of the fruit, it may actually repress transcription during later fruit maturation stages to balance anthocyanin content.[60] A conserved network of transcriptional activators (DPL, PHZ, and AN1) and repressors (MYB27 and MYBx) regulate anthocyanin pigmentation in eudicots. PhMYB27 is orthologous to FaMYB1 and was shown to be repressed under bright light but highly expressed under shaded conditions. Furthermore, being part of the MBW complex, it acts on PhAN1 as well as genes involved in anthocyanin biosynthesis through its C-terminal EAR motif,

thereby suppressing transcription. PhAN1 is also targeted PhMYBx, competitive R3-MYB repressor which inhibits PhAN1 activity; overall, the ability of the MBW complex to inhibit and activate PhAN1, PhMYB27, and PhMYBx provides both reinforcement and feedback regulation.[59,61] Similarly, in tomato, the R3-MYB repressor *SlMYBL2* was significantly upregulated in Pro35S: BrTT8 seedlings by the MBW complex itself under high light. However, at the same time, it could also bind competitively with the MYB interaction domain of BrTT8 to inhibit anthocyanin biosynthesis, leading to restricted anthocyanin production.[62]

Identification of these repressors and elucidation of the network of activators and repressors regulating the synthesis of flavonoids in other plant species have raised renewed interest. In our work, *StMYB3* and *StMYBATV* were identified as highly correlated with flavonoid accumulation, and they are the orthologous genes of *PhMYB27* and *PhMYBx*. It was assumed that they may act in the negative feedback regulation mechanism on anthocyanin biosynthesis as it is the case for PhMYB27 and PhMYBx.[59] *StMYB3* and *StMYBATV* are highly expressed at the tuber pigmentation stage (Figure 6); this is consistent with what was observed for MYB repressors involved in anthocyanin biosynthesis in other species. In contrast, while potato white skin displays high expression of *StMYB113*, *StMYBA1*, and *StAN1*, the *bHLH* partners' expression levels appeared to be constrained, thus indicating that bHLHs could be critical for regulating the synthesis of anthocyanins in potato.[57] We hypothesize that StMYB3 and StMYBATV could form complexes with StbHLH1 to prevent the MBW complex from being formed, thus preventing it from interacting with the R2R3-MYB activator, leading to restricted anthocyanin production (Figure 9). This hypothesis is in line with our results that the interaction of StMYB3 and StMYBATV with the anthocyanin promoting StbHLH1, the inhibition of anthocyanin production in tobacco (*N. tabacum*), and the inhibition of *DFR* promotor activation in *Nicotiana benthemiana* leaves where StMYB3, StMYBATV, and StAN1 with StbHLH1 were transiently co-expressed (Figure 8). The *StMYB3* and *StMYBATV* may be activated by the MBW complex itself and/or other unknown proteins under certain developmental stages. There was no significant difference of *StAN1* expression in the flesh of R at three stages, but the *StbHLH1* transcript was significantly higher in red flesh of R at the S3 stage than that in yellow flesh of R at the S2 stage, suggesting *StMYB3* and *StMYBATV* might be activated by StbHLH1 or other unknown proteins, rather than StAN1, which requires further investigation.

In conclusion, we explored the regulatory network connected to flavonoid biosynthesis using targeted metabolome and transcriptome analysis in different potato clones during development. Five modules were identified that positively or negatively correlated with flavonoid accumulation. The provided candidate genes for potato anthocyanin, flavone, and flavonol accumulation can guide future functional studies. Two MYB repressors involved in flavonoid biosynthesis during potato tuber pigmentation were functionally identified, suggesting a feedback regulatory mechanism underlying the biosynthesis of flavonoid accumulation in colored potatoes during tuber development.

Limitations of the study

This work revealed a dynamic regulatory mechanism of potato tuber pigmentation: (1) a total of 72 flavonoids were identified in pigmented flesh; (2) the candidate genes that positively or negatively regulate flavonoid biosynthesis were identified based on WGCNA analysis; (3) two MYB repressors (an R2R3-MYB StMYB3 and an R3-MYB StMYBATV) were determined engaged in feedback regulatory mechanisms. Although the function and regulatory mechanism of StMYB3 and StMYBATV on anthocyanin biosynthesis have been preliminarily determined based on yeast two-hybrid assay, transient assay, and BiFC assay, further verification of their function in potato tuber via stable genetic transformation of potato using overexpression, RNAi, and CRISPR/Cas9 systems is needed. The detailed mechanism needs to be further explored.

STAR★METHODS

Detailed methods are provided in the online version of this paper and include the following:

- KEY RESOURCES TABLE
- RESOURCE AVAILABILITY
  - Lead contact
  - Materials availability
  - Data and code availability

SUPPLEMENTAL INFORMATION

Supplemental information can be found online at https://doi.org/10.1016/j.isci.2022.105903.

ACKNOWLEDGMENTS

The Research Program was sponsored by the National Natural Science Foundation of China (31860398), the Key Program of Gansu Natural Science Foundation (22JR5RA834), the Major S&T Special Projects of Gansu Province (22ZD6NA010), the Fuxi Talent Project of Gansu Agricultural University (Gaufx-02Y04), and the Earmarked Fund for China Agriculture Research System (CARS-09-P14). We would like to thank Pro. Richard V. Espley and Pro. Andrew C. Allan (The New Zealand Institute for Plant and Food Research Limited, New Zealand) for the suggestions and help on the paper. We also would like to thank Pro. Pu Yan (Institute of Tropical Bioscience and Biotechnology, Chinese Academy of Tropical Agricultural Sciences, China) for having provided plasmids and technical advice.

AUTHOR CONTRIBUTIONS

YL and ZL: devising the experiment, statistical analysis, and writing; YL, LW, and JZ: data collection; KLW: data analysis and revision; ZB and CS: conceptualization; JZ and JB: supervision. All authors reviewed and edited the final manuscript.

DECLARATION OF INTERESTS

The authors declare no competing interests.

INCLUSION AND DIVERSITY

We support inclusive, diverse, and equitable conduct of research.

Received: August 10, 2022
Revised: November 12, 2022
Accepted: December 26, 2022
Published: December 29, 2022

REFERENCES

1. He, J., and Giusti, M.M. (2010). Anthocyanins: natural colorants with health-promoting properties. Annu. Rev. Food Sci. Technol. *1*, 163–187. https://doi.org/10.1146/annurev.food.080708.100754.

2. Jansen, G., and Flamme, W. (2006). Coloured potatoes (*Solanum Tuberosum* L.) - anthocyanin content and tuber quality. Genet. Resour. Crop Evol. *53*, 1321–1331. https://doi.org/10.1007/s10722-005-3880-2.

3. Jaakola, L. (2013). New insights into the regulation of anthocyanin biosynthesis in fruits. Trends Plant Sci. *18*, 477–483. https://doi.org/10.1016/j.tplants.2013.06.003.

4. Goodman, C.D., Casati, P., and Walbot, V. (2004). A multidrug resistance-associated protein involved in anthocyanin transport in *Zea mays*. Plant Cell *16*, 1812–1826. https://doi.org/10.1105/tpc.022574.

5. Marinova, K., Pourcel, L., Weder, B., Schwarz, M., Barron, D., Routaboul, J.M., Debeaujon, I., and Klein, M. (2007). The *Arabidopsis* MATE transporter TT12 acts as a vacuolar flavonoid/H+ -antiporter active in proanthocyanidin-accumulating cells of the seed coat. Plant Cell *19*, 2023–2038. https://doi.org/10.1105/tpc.106.046029.

6. Mueller, L.A., Goodman, C.D., Silady, R.A., and Walbot, V. (2000). AN9, a petunia glutathione S-transferase required for anthocyanin sequestration, is a flavonoid-binding protein. Plant Physiol. *123*, 1561–1570. https://doi.org/10.1104/pp.123.4.1561.

7. Zhao, J. (2015). Flavonoid transport mechanisms: how to go, and with whom. Trends Plant Sci. *20*, 576–585. https://doi.org/10.1016/j.tplants.2015.06.007.

8. Koes, R., Verweij, W., and Quattrocchio, F. (2005). Flavonoids: a colorful model for the regulation and evolution of biochemical pathways. Trends Plant Sci. *10*, 236–242. https://doi.org/10.1016/j.tplants.2005.03.002.

9. Patra, B., Schluttenhofer, C., Wu, Y., Pattanaik, S., and Yuan, L. (2013). Transcriptional regulation of secondary metabolite biosynthesis in plants. Biochim. Biophys. Acta *1829*, 1236–1247. https://doi.org/10.1016/j.bbagrm.2013.09.006.

10. Hichri, I., Barrieu, F., Bogs, J., Kappel, C., Delrot, S., and Lauvergeat, V. (2011). Recent advances in the transcriptional regulation of the flavonoid biosynthetic pathway. J. Exp. Bot. *62*, 2465–2483. https://doi.org/10.1093/jxb/erq442.

11. Stracke, R., Ishihara, H., Huep, G., Barsch, A., Mehrtens, F., Niehaus, K., and Weisshaar, B. (2007). Differential regulation of closely related R2R3-MYB transcription factors controls flavonol accumulation in different parts of the *Arabidopsis thaliana* seedling. Plant J. *50*, 660–677. https://doi.org/10.1111/j.1365-313X.2007.03078.x.

12. Xu, W., Dubos, C., and Lepiniec, L. (2015). Transcriptional control of flavonoid biosynthesis by MYB-bHLH-WDR complexes. Trends Plant Sci. *20*, 176–185. https://doi.org/10.1016/j.tplants.2014.12.001.

13. Dubos, C., Stracke, R., Grotewold, E., Weisshaar, B., Martin, C., and Lepiniec, L. (2010). MYB transcription factors in *Arabidopsis*. Trends Plant Sci. *15*, 573–581. https://doi.org/10.1016/j.tplants.2010.06.005.

14. Stracke, R., Jahns, O., Keck, M., Tohge, T., Niehaus, K., Fernie, A.R., and Weisshaar, B. (2010). Analysis of PRODUCTION OF FLAVONOL GLYCOSIDES-dependent flavonol glycoside accumulation in *Arabidopsis thaliana* plants reveals MYB11-MYB12-and MYB111-independent flavonol glycoside accumulation. New Phytol. *188*, 985–1000. https://doi.org/10.1111/j.1469-8137.2010.03421.x.

15. Xu, W., Grain, D., Bobet, S., Le Gourrierec, J., Thévenin, J., Kelemen, Z., Lepiniec, L., and Dubos, C. (2014). Complexity and robustness of the flavonoid transcriptional regulatory network revealed by comprehensive analyses of MYB-bHLH-WDR complexes and their targets in *Arabidopsis* seed. New Phytol. *202*, 132–144. https://doi.org/10.1111/nph.12620.

16. Azuma, A., Kobayashi, S., Mitani, N., Shiraishi, M., Yamada, M., Ueno, T., Kono, A., Yakushiji, H., and Koshita, Y. (2008). Genomic and genetic analysis of Myb-related genes that regulate anthocyanin biosynthesis in grape berry skin. Theor. Appl. Genet. *117*, 1009–1019. https://doi.org/10.1007/s00122-008-0840-1.

17. Jung, C.S., Griffiths, H.M., De Jong, D.M., Cheng, S., Bodis, M., Kim, T.S., and De Jong, W.S. (2009). The potato *developer* (*D*) locus encodes an R2R3 MYB transcription factor that regulates expression of multiple anthocyanin structural genes in tuber skin. Theor. Appl. Genet. *120*, 45–57. https://doi.org/10.1007/s00122-009-1158-3.

18. Liu, Y., Lin-Wang, K., Espley, R.V., Wang, L., Yang, H., Yu, B., Dare, A., Varkonyi-Gasic, E., Wang, J., Zhang, J., et al. (2016). Functional diversification of the potato R2R3 MYB anthocyanin activators AN1, MYBA1, and MYB113 and their interaction with basic helix-loop-helix cofactors. J. Exp. Bot. *67*, 2159–2176. https://doi.org/10.1093/jxb/erw014.

19. Gonzalez, A., Zhao, M., Leavitt, J.M., and Lloyd, A.M. (2008). Regulation of the anthocyanin biosynthetic pathway by the TTG1/bHLH/Myb transcriptional complex in *Arabidopsis* seedlings. Plant J. *53*, 814–827. https://doi.org/10.1111/j.1365-313X.2007.03373.x.

20. Espley, R.V., Hellens, R.P., Putterill, J., Stevenson, D.E., Kutty-Amma, S., and Allan, A.C. (2007). Red colouration in apple fruit is due to the activity of the MYB transcription factor, MdMYB10. Plant J. *49*, 414–427. https://doi.org/10.1111/j.1365-313X.2006.02964.x.

21. Chagné, D., Lin-Wang, K., Espley, R.V., Volz, R.K., How, N.M., Rouse, S., Brendolise, C., Carlisle, C.M., Kumar, S., De Silva, N., et al. (2013). An ancient duplication of apple MYB transcription factors is responsible for novel red fruit-flesh phenotypes. Plant Physiol. *161*, 225–239. https://doi.org/10.1104/pp.112.206771.

22. Jin, H., Cominelli, E., Bailey, P., Parr, A., Mehrtens, F., Jones, J., Tonelli, C., Weisshaar, B., and Martin, C. (2000). Transcriptional repression by AtMYB4 controls production of UV-protecting sunscreens in *Arabidopsis*. EMBO J. *19*, 6150–6161. https://doi.org/10.1093/emboj/19.22.6150.

23. Dubos, C., Le Gourrierec, J., Baudry, A., Huep, G., Lanet, E., Debeaujon, I., Routaboul, J.M., Alboresi, A., Weisshaar, B., and Lepiniec, L. (2008). MYBL2 is a new regulator of flavonoid biosynthesis in *Arabidopsis thaliana*. Plant J. *55*, 940–953. https://doi.org/10.1111/j.1365-313X.2008.03564.x.

24. Nesi, N., Debeaujon, I., Jond, C., Stewart, A.J., Jenkins, G.I., Caboche, M., and Lepiniec, L. (2002). The TRANSPARENT TESTA16 locus encodes the ARABIDOPSIS BSISTER MADS domain protein and is required for proper development and pigmentation of the seed coat. Plant Cell *14*, 2463–2479. https://doi.org/10.1105/tpc.004127.

25. Sagasser, M., Lu, G.H., Hahlbrock, K., and Weisshaar, B. (2002). *A. thaliana* TRANSPARENT TESTA 1 is involved in seed coat development and defines the WIP subfamily of plant zinc finger proteins. Genes Dev. *16*, 138–149. https://doi.org/10.1101/gad.212702.

26. Cheng, Y., Liu, L., Yuan, C., and Guan, J. (2016). Molecular characterization of ethylene-regulated anthocyanin biosynthesis in plums during fruit ripening. Plant Mol. Biol. Rep. *34*, 777–785. https://doi.org/10.1007/s11105-015-0963-x.

27. Ishida, T., Hattori, S., Sano, R., Inoue, K., Shirano, Y., Hayashi, H., Shibata, D., Sato, S., Kato, T., Tabata, S., et al. (2007). *Arabidopsis TRANSPARENT TESTA GLABRA2* is directly regulated by R2R3 MYB transcription factors and is involved in regulation of *GLABRA2* transcription in epidermal differentiation. Plant Cell *19*, 2531–2543. https://doi.org/10.1105/tpc.107.052274.

28. Mao, Z., Jiang, H., Wang, S., Wang, Y., Yu, L., Zou, Q., Liu, W., Jiang, S., Wang, N., Zhang, Z., and Chen, X. (2021). The MdHY5-MdWRKY41-MdMYB transcription factor cascade regulates the anthocyanin and proanthocyanidin biosynthesis in red-fleshed apple. Plant Sci. *306*, 110848. https://doi.org/10.1016/j.plantsci.2021.110848.

29. An, J.P., Qu, F.J., Yao, J.F., Wang, X.N., You, C.X., Wang, X.F., and Hao, Y.J. (2017). The bZIP transcription factor $MdHY_5$ regulates anthocyanin accumulation and nitrate assimilation in apple. Hortic. Res. *4*, 17056. https://doi.org/10.1038/hortres.2017.56.

30. Hartmann, U., Sagasser, M., Mehrtens, F., Stracke, R., and Weisshaar, B. (2005). Differential combinatorial interactions of cis-acting elements recognized by R2R3-MYB, BZIP, and BHLH factors control light-responsive and tissue-specific activation of phenylpropanoid biosynthesis genes. Plant Mol. Biol. *57*, 155–171. https://doi.org/10.1007/s11103-004-6910-0.

31. Yao, G., Ming, M., Allan, A.C., Gu, C., Li, L., Wu, X., Wang, R., Chang, Y., Qi, K., Zhang, S., and Wu, J. (2017). Map-based cloning of the pear gene MYB114 identifies an interaction with other transcription factors to coordinately regulate fruit anthocyanin biosynthesis. Plant J. *92*, 437–451. https://doi.org/10.1111/tpj.13666.

32. Zhou, H., Lin-Wang, K., Wang, H., Gu, C., Dare, A.P., Espley, R.V., He, H., Allan, A.C., and Han, Y. (2015). Molecular genetics of blood-fleshed peach reveals activation of anthocyanin biosynthesis by NAC transcription factors. Plant J. *82*, 105–121. https://doi.org/10.1111/tpj.12792.

33. Jung, C.S., Griffiths, H.M., De Jong, D.M., Cheng, S., Bodis, M., and De Jong, W.S. (2005). The potato *P* locus codes for flavonoid 3′, 5′-hydroxylase. Theor. Appl. Genet. *110*, 269–275. https://doi.org/10.1007/s00122-004-1829-z.

34. Zhang, Y., Cheng, S., De Jong, D., Griffiths, H., Halitschke, R., and De Jong, W. (2009). The potato *R* locus codes for dihydroflavonol 4-reductase. Theor. Appl. Genet. *119*, 931–937. https://doi.org/10.1007/s00122-009-1100-8.

35. Zhang, Y., Jung, C.S., and De Jong, W.S. (2009). Genetic analysis of pigmented tuber flesh in potato. Theor. Appl. Genet. *119*, 143–150. https://doi.org/10.1007/s00122-009-1024-3.

36. De Jong, H. (1987). Inheritance of pigmented tuber flesh in cultivated diploid potatoes. Am. Potato J. *64*, 337–343. https://doi.org/10.1007/bf02853595.

37. Rommens, C.M., Richael, C.M., Yan, H., Navarre, D.A., Ye, J., Krucker, M., and Swords, K. (2008). Engineered native pathways for high kaempferol and caffeoylquinate production in potato. Plant Biotechnol. J. *6*, 870–886. https://doi.org/10.1111/j.1467-7652.2008.00362.x.

38. Stushnoff, C., Ducreux, L.J.M., Hancock, R.D., Hedley, P.E., Holm, D.G., Mcdougall, G.J., Mcnicol, J.W., Morris, J., Morris, W.L., Sungurtas, J.A., et al. (2010). Flavonoid profiling and transcriptome analysis reveals new gene-metabolite correlations in tubers of *Solanum tuberosum* L. J. Exp. Bot. *61*, 1225–1238. https://doi.org/10.1093/jxb/erp394.

39. Cho, K., Cho, K.S., Sohn, H.B., Ha, I.J., Hong, S.Y., Lee, H., Kim, Y.M., and Nam, M.H. (2016). Network analysis of the metabolome and transcriptome reveals novel regulation of potato pigmentation. J. Exp. Bot. *67*, 1519–1533. https://doi.org/10.1093/jxb/erv549.

40. Bonar, N., Liney, M., Zhang, R., Austin, C., Dessoly, J., Davidson, D., Stephens, J., McDougall, G., Taylor, M., Bryan, G.J., and Hornyik, C. (2018). Potato miR828 is associated with purple tuber skin and flesh color. Front. Plant Sci. *9*, 1742. https://doi.org/10.3389/fpls.2018.01742.

41. D'Amelia, V., Aversano, R., Batelli, G., Caruso, I., Castellano Moreno, M., Castro-Sanz, A.B., Chiaiese, P., Fasano, C., Palomba, F., and Carputo, D. (2014). High AN1 variability and interaction with basic helix-loop-helix co-factors related to anthocyanin biosynthesis in potato leaves. Plant J. *80*, 527–540. https://doi.org/10.1111/tpj.12653.

42. D'Amelia, V., Villano, C., Batelli, G., Çobanoğlu, Ö., Carucci, F., Melito, S., Chessa, M., Chiaiese, P., Aversano, R., and Carputo, D. (2020). Genetic and epigenetic dynamics affecting anthocyanin biosynthesis in potato cell culture. Plant Sci. *298*, 110597. https://doi.org/10.1016/j.plantsci.2020.110597.

43. Liu, Y., Lin-Wang, K., Espley, R.V., Wang, L., Li, Y., Liu, Z., Zhou, P., Zeng, L., Zhang, X., Zhang, J., and Allan, A.C. (2019). StMYB44 negatively regulates anthocyanin biosynthesis at high temperatures in tuber flesh of potato. J. Exp. Bot. *70*, 3809–3824. https://doi.org/10.1093/jxb/erz194.

44. Langfelder, P., and Horvath, S. (2008). WGCNA: an R package for weighted correlation network analysis. BMC Bioinformatics *9*, 559. https://doi.org/10.1186/1471-2105-9-559.

45. Shannon, P., Markiel, A., Ozier, O., Baliga, N.S., Wang, J.T., Ramage, D., Amin, N., Schwikowski, B., and Ideker, T. (2003). Cytoscape: a software environment for integrated models of biomolecular interaction networks. Genome Res. *13*, 2498–2504. https://doi.org/10.1101/gr.1239303.

46. Tian, J., Han, Z.Y., Zhang, J., Hu, Y., Song, T., and Yao, Y. (2015). The balance of expression of dihydroflavonol 4-reductase and flavonol synthase regulates flavonoid biosynthesis and red foliage coloration in crabapples. Sci. Rep. *5*, 12228. https://doi.org/10.1038/srep12228.

47. Hammerbacher, A., Paetz, C., Wright, L.P., Fischer, T.C., Bohlmann, J., Davis, A.J., Fenning, T.M., Gershenzon, J., and Schmidt, A. (2014). Flavan-3-ols in Norway Spruce: biosynthesis, accumulation, and function in response to attack by the bark beetle-associated fungus *Ceratocystis polonica*. Plant Physiol. *164*, 2107–2122. https://doi.org/10.1104/pp.113.232389.

48. Baxter, I.R., Young, J.C., Armstrong, G., Foster, N., Bogenschutz, N., Cordova, T., Peer, W.A., Hazen, S.P., Murphy, A.S., and Harper, J.F. (2005). A plasma membrane H+-ATPase is required for the formation of proanthocyanidins in the seed coat endothelium of *Arabidopsis thaliana*. Proc. Natl. Acad. Sci. USA *102*, 2649–2654. https://doi.org/10.1073/pnas.0406377102.

49. Stracke, R., Werber, M., and Weisshaar, B. (2001). The R2R3-MYB gene family in *Arabidopsis thaliana*. Curr. Opin. Plant Biol. *4*, 447–456. https://doi.org/10.1016/s1369-5266(00)00199-0.

50. D'Amelia, V., Staiti, A., D'Orso, F., Maisto, M., Piccolo, V., Aversano, R., and Carputo, D. (2022). Targeted mutagenesis of *StISAC* stabilizes the production of anthocyanins in potato cell culture. Plant Direct *6*, e433. https://doi.org/10.1002/pld3.433.

51. Wang, S., and Chen, J.G. (2014). Regulation of cell fate determination by single-repeat R3 MYB transcription factors in *Arabidopsis*. Front. Plant Sci. *5*, 133. https://doi.org/10.3389/fpls.2014.00133.

52. Crowe, F.L., Roddam, A.W., Key, T.J., Appleby, P.N., Overvad, K., Jakobsen, M.U., Tjønneland, A., Hansen, L., Boeing, H., Weikert, C., et al. (2011). Fruit and vegetable intake and mortality from ischaemic heart disease: results from the European Prospective Investigation into Cancer and Nutrition (EPIC)-Heart study. Eur. Heart J. *32*, 1235–1243. https://doi.org/10.1093/eurheartj/ehq465.

53. Ramsay, N.A., and Glover, B.J. (2005). MYB-bHLH-WD40 protein complex and the evolution of cellular diversity. Trends Plant Sci. *10*, 63–70. https://doi.org/10.1016/j.tplants.2004.12.011.

54. Liu, Y., Tikunov, Y., Schouten, R.E., Marcelis, L.F.M., Visser, R.G.F., and Bovy, A. (2018). Anthocyanin biosynthesis and degradation mechanisms in *Solanaceous* vegetables: a review. Front. Chem. *6*, 52. https://doi.org/10.3389/fchem.2018.00052.

55. Strygina, K.V., Kochetov, A.V., and Khlestkina, E.K. (2019). Genetic control of anthocyanin pigmentation of potato tissues. BMC Genet. *20*, 27–43. https://doi.org/10.1186/s12863-019-0728-x.

56. Tengkun, N., Dongdong, W., Xiaohui, M., Yue, C., and Qin, C. (2019). Analysis of key genes involved in potato anthocyanin biosynthesis based on genomics and transcriptomics data. Front. Plant Sci. *10*, 603. https://doi.org/10.3389/fpls.2019.00603.

57. Payyavula, R.S., Singh, R.K., and Navarre, D.A. (2013). Transcription factors, sucrose, and sucrose metabolic genes interact to regulate potato phenylpropanoid metabolism. J. Exp. Bot. *64*, 5115–5131. https://doi.org/10.1093/jxb/ert303.

58. Dey, A., Samanta, M.K., Gayen, S., and Maiti, M.K. (2016). The sucrose non-fermenting 1-related kinase 2 gene *SAPK9* improves drought tolerance and grain yield in rice by modulating cellular osmotic potential, stomatal closure and stress-responsive gene expression. BMC Plant Biol. *16*, 158. https://doi.org/10.1186/s12870-016-0845-x.

59. Albert, N.W., Davies, K.M., Lewis, D.H., Zhang, H., Montefiori, M., Brendolise, C., Boase, M.R., Ngo, H., Jameson, P.E., and Schwinn, K.E. (2014). A conserved network of transcriptional activators and repressors regulates anthocyanin pigmentation in eudicots. Plant Cell *26*, 962–980. https://doi.org/10.1105/tpc.113.122069.

60. Aharoni, A., De Vos, C.H., Wein, M., Sun, Z., Greco, R., Kroon, A., Mol, J.N., and O'Connell, A.P. (2001). The strawberry FaMYB1 transcription factor suppresses anthocyanin and flavonol accumulation in transgenic tobacco. Plant J. *28*, 319–332. https://doi.org/10.1046/j.1365-313x.2001.01154.x.

61. Albert, N.W., Lewis, D.H., Zhang, H., Schwinn, K.E., Jameson, P.E., and Davies, K.M. (2011). Members of an R2R3-MYB transcription factor family in *Petunia* are developmentally and environmentally regulated to control complex floral and vegetative pigmentation patterning. Plant J. *65*, 771–784. https://doi.org/10.1111/j.1365-313X.2010.04465.x.

62. Zhang, Y., Li, Y., Li, W., Hu, Z., Yu, X., Tu, Y., Zhang, M., Huang, J., and Chen, G. (2019). Metabolic and molecular analysis of nonuniform anthocyanin pigmentation in tomato fruit under high light. Hortic. Res. *6*, 56. https://doi.org/10.1038/s41438-019-0138-2.

63. Yan, P., Zeng, Y., Shen, W., Tuo, D., Li, X., and Zhou, P. (2019). Nimble cloning: a simple, versatile, and efficient system for standardized molecular cloning. Front. Bioeng. Biotechnol. *7*, 460. https://doi.org/10.3389/fbioe.2019.00460.

64. Love, M.I., Huber, W., and Anders, S. (2014). Moderated estimation of fold change and dispersion for RNA-Seq data with DESeq2. Genome Biol. *15*, 550. https://doi.org/10.1186/s13059-014-0550-8.

65. Chen, C., Chen, H., Zhang, Y., Thomas, H.R., Frank, M.H., He, Y., and Xia, R. (2020). TBtools: An integrative toolkit developed for interactive analyses of big biological data. Mol Plant. *13*, 1194–1202. https://doi.org/10.1016/j.molp.2020.06.009.

66. Chen, W., Gong, L., Guo, Z., Wang, W., Zhang, H., Liu, X., Yu, S., Xiong, L., and Luo, J. (2013). A novel integrated method for large-scale detection, identification, and quantification of widely targeted metabolites: application in the study of rice metabolomics. Mol. Plant *6*, 1769–1780. https://doi.org/10.1093/mp/sst080.

67. Wang, A., Li, R., Ren, L., Gao, X., Zhang, Y., Ma, Z., Ma, D., and Luo, Y. (2018). A comparative metabolomics study of flavonoids in sweet potato with different flesh colors (*Ipomoea batatas* (L.) Lam). Food Chem. *260*, 124–134. https://doi.org/10.1016/j.foodchem.2018.03.125.

68. Pham, G.M., Hamilton, J.P., Wood, J.C., Burke, J.T., Zhao, H., Vaillancourt, B., Ou, S., Jiang, J., and Buell, C.R. (2020). Construction of a chromosome-scale long-read reference genome assembly for potato. GigaScience *9*, giaa100. https://doi.org/10.1093/gigascience/giaa100.

69. Espley, R.V., Brendolise, C., Chagné, D., Kutty-Amma, S., Green, S., Volz, R., Putterill, J., Schouten, H.J., Gardiner, S.E., Hellens, R.P., and Allan, A.C. (2009). Multiple repeats of a promoter segment causes transcription factor autoregulation in red apples. Plant Cell *21*, 168–183. https://doi.org/10.1105/tpc.108.059329.

70. Hellens, R.P., Allan, A.C., Friel, E.N., Bolitho, K., Grafton, K., Templeton, M.D., Karunairetnam, S., Gleave, A.P., and Laing, W.A. (2005). Transient expression vectors for functional genomics, quantification of promoter activity and RNA silencing in plants. Plant Methods *1*, 13. https://doi.org/10.1186/1746-4811-1-13.

71. Tang, X., Zhang, N., Si, H., and Calderón-Urrea, A. (2017). Selection and validation of reference genes for RT-qPCR analysis in potato under abiotic stress. Plant Methods *13*, 85. https://doi.org/10.1186/s13007-017-0238-7.

STAR★METHODS

KEY RESOURCES TABLE

REAGENT or RESOURCE	SOURCE	IDENTIFIER
Bacterial and virus strains		
Agrobacterium tumefaciens strains GV3101	Shanghai Weidi Biotechnology	AC1030S
Biological samples		
Solanum tuberosum genotypes : CIP 302281.17, CIP 302281.25, CIP 302281.15	This study	N/A
Critical commercial assays		
PureLink Plant RNA Reagent Kit	Invitrogen	CAT#12183018A
Platinum Taq DNA Polymerase High Fidelity	Invitrogen	CAT#10966018
SuperReal Pre-Mix Plus	TIANGEN	CAT#FP205
Dual-Luciferase Reporter Assay System	Promega	CAT#E1910
Deposited data		
KEGG database	KEGG	https://www.genome.jp/kegg/pathway.html
Raw Data for RNA-seq	This study	GenBank: PRJNA782081
Oligonucleotides		
Gene specific primers for qRT-PCR analysis and full length cloning, see Table S1	This study	N/A
Recombinant DNA		
pNC-Cam2304-MCS35S	(Yan et al., 2019)[63]	N/A
pGreenII 0800-LUC-*prom-3-StDFR*	(Liu et al., 2016)[18]	N/A
pSAK277-*StAN1-R1*	(Liu et al., 2016)[18]	N/A
pSAK277-*StbHLH1*	(Liu et al., 2016)[18]	N/A
pNC-Cam2304-MCS35S-*MYBATV*	This study	N/A
pNC-Cam2304-MCS35S-*MYB3*	This study	N/A
pNC-GADT7 (AD-EV, AD-*StAN1*, AD-*StMYB3*, and AD-*StMYBATV*)	This study	N/A
pNC-GBKT7 (BD-*StbHLH1*)	This study	N/A
pNC-BiFC-Enn-(*StAN1*/*StMYB3*/*StMYBATV*)	This study	N/A
pNC-BiFC-Ecn-*StbHLH1*	This study	N/A
Software and algorithms		
R v 3.6.3	R Core Team 2020	https://www.r-project.org/
DESeq2 v1.34.0	(Love et al., 2014)[64]	https://bioconductor.org/packages/release/bioc/html/DESeq2.html
TBtools	(Chen et al., 2020)[65]	https://github.com/CJ-Chen/TBtools
Cytoscape	(Shannon et al., 2003)[45]	https://cytoscape.org
Other		
CFX96 Touch Real-Time PCR Detection System	Bio-Rad	CFX96
HiSeq 4000 Sequencing System	Metware Biotechnology	N/A
UPLC-ESI-MS/MS	Metware Biotechnology	N/A

RESOURCE AVAILABILITY

Lead contact

Further information and requests for resources should be directed to and will be fulfilled by the lead contact Jiangping Bai (baijp@gsau.edu.cn).

Materials availability

Plasmids generated in this study are available from the lead contact upon request.

Data and code availability

The datasets generated in this study have been deposited in the Sequence Read Archive (SRA), the accession number is listed in the key resources table.Other data supporting our findings are available within the paper and its Supplementary Information files.

EXPERIMENTAL MODEL AND SUBJECT DETAILS

Plant material and sampling

Three potato clones (yellow clone – CIP 302281.17, red clone – CIP 302281.25, and purple clone – CIP 302281.15) derived from the same parentage were acquired from Hebei North University and grown in field conditions at Dingxi Academy of Agricultural Science, Gansu Province. The dominant flesh color of the yellow clone transformed from white to pale yellow and then to yellow over development. On the other hand, the red and purple clones, changed from white/pale yellow/red to pale purple/purple/dark purple during the three developmental stages. These were abbreviated to Y, R, and P. The tuber flesh of the three potato clones was collected at the tuberization stage (S1), tuber bulking stage (S2), and tuber maturation stage (S3) (100, 130, 170 days after sowing). The flesh tissue inside the vascular ring of five tubers was collected from each potato clone and at each time point before being pooled, with samples collected from three individual plants used as three biological replicates. After collection, liquid nitrogen was used to immediately freeze samples prior to storage at −80°C.

METHOD DETAILS

Widely targeted metabolic profiling and data analysis

Sample preparation and extraction

Metabolomic analyses were carried out by Metware Biotechnology Co., Ltd (Wuhan, China), as described before.[66,67] In brief, after freeze-drying (Scientz - 100F, Scientz, China), each potato tuber was ground into powder at 30 Hz and for 1.5 min with the help of a mixer mill (MM 400, Retsch, Germany) containing zirconia beads. The resulting powder (100 mg) was dissolved in 1.2 mL of 70% aqueous methanol, vortexed six times (once every half an hour for 30 s) and stored overnight at 4°C. This was followed by centrifugation for 10 min at 12000 rpm and after filtration (SCAA-104, 0.22 μm pore size; ANPEL, Shanghai, China), samples were analyzed by UPLC-MS/MS.

UPLC conditions

For sample analysis with an UPLC-ESI-MS/MS system (UPLC, SHIMADZU NexeraX2; MS, Applied Biosystems 4500 Q TRAP), an Agilent SB-C18 column (1.8 μm, 2.1 mm*100 mm) was used, with mobile phases A and B consisting of pure water with 0.1% of formic acid and acetonitrile with 0.1% of formic acid (v/v) respectively. A temperature of 40°C, a flow rate of 0.35 mL/min as well as an injection volume of 4 μL were also selected as additional parameters. A gradient elution was applied, starting with 95% of A and 5% of B. Within 9 min, 5% of A and 95% of B was selected as a linear gradient and maintained for 1min before switching to 95% of A and 5% of B within 1.1 min. This final gradient was maintained for 2.9 min. Analysis of eluted samples was subsequently performed with an ESI-triple quadrupole-linear ion trap (QTRAP) - MS.

ESI-Q TRAP-MS/MS

A triple quadruple-linear ion trap mass spectrometer (QTRAP, AB4500 Q TRAP UPLC/MS/MS System) to which an ESI Turbo Ion-Spray interface was connected, was used to acquire linear ion trap (LIT) and triple quadruple (QQQ) scans. The spray, controlled by the Analyst 1.6.3 software (ABSciex), was operated in positive and negative ion modes and under the following conditions: a source temperature of 550°C; turbo spray; ion source; a high collisionally-activated dissociation (CAD); pressures of 25, 50 and 60 psi for curtain gas (CUR) as well as ion source gases I (GSI) and II (GSII), respectively; an ion spray voltage (IS) of 5500V and −4500V for positive ion and negative ion modes respectively. Mass calibration and instrument tuning was carried out with polypropylene glycol solutions at concentrations of 10 and 100 μmol/L in QQQ and LIT modes respectively. QQQ scans were acquired as multiple reaction monitoring (MRM) experiments with nitrogen, as the collision gas, set to medium. Collision energy (CE) and Declustering potential (DP) for

individual MRM transitions was done after additional optimization of CE and DP. A specific set of MRM transitions was monitored for each period depending on the eluents within this period.

Metabolomics analysis

As described in other studies, the metabolic profile was determined using the self-built database MWDB (Metware biotechnology Co., Ltd. Wuhan, China).[66,67] MS data were qualitatively analyzed by comparing fragmentation patterns, retention times (RTs) as well as precursor ion (Q1) and production (Q3) values with the results obtained when using standards (Sigma-Aldrich,USA) under the same conditions. Moreover, the MRM mode was used for quantifying metabolites. For this purpose, signal strengths were first acquired by screening the ions for each metabolite through QQQ MS, with the area under chromatographic peaks subsequently indicating relative metabolite content. In addition, metabolites that were differentially produced between samples were screened and quantified using metaX software (http://metax.genomics.cn/), with an absolute $\log_2$FC (fold change) ≥ 1 and a VIP (variable importance in project) value ≥ 1 selected as thresholds for classifying metabolites as being differentially regulated between groups. VIP values were extracted from OPLS-DA result, which also include permutation plots and score plots, was obtained by using R package MetaboAnalystR. For the identified metabolites, principal component analysis (PCA) and orthogonal partial least squares discriminant analysis (OPLS-DA) were then performed in R (www.r-project.org/) before mapping these differential metabolites onto the Kyoto Encyclopedia of Genes and Genomes (KEGG) database (http://www.kegg.jp/kegg/pathway.html). All experiments were carried out with triplicate samples.

RNA extraction, library construction and sequencing

The PureLink Plant RNA Reagent Kit (Invitrogen, USA) was used as specified by the manufacturer for total RNA extraction from the tuber flesh of three potato clones at three developmental stages. RNA quality and quantity were then determined by electrophoresis (1% agarose gel) as well as with a Nanodrop ND-1000 spectrophotometer (Nanodrop Technologies, USA) and a Qubit 2.0 Fluorometer (Life Technologies, USA). Using the RNA Nano 6000 Assay Kit, the integrity of the extracted RNA was also assessed on an Agilent Bioanalyzer 2100 (Agilent Technologies, USA).

Messenger RNAs (mRNAs), purified from the total RNA with the help of a Dynabeads mRNA Purification Kit (Invitrogen, USA), were fragmented before using random hexamer primers to synthesize a first cDNA strand by reverse-transciption. This was followd by the synthesis of a second strand using DNA Polymerase I, dNTPs and buffer. Double-stranded cDNAs, purified with AMPure XP beads, were repaired at the ends, poly-A-tails as well as adaptors were ligated, and fragment size selection was carried out through AMPure XP beads. Finally, cDNA libraries were generated by PCR enrichment prior to sequencing on an Illumina HiSeq platform by MetWare Biotechnology Co. Ltd (Wuhan, China).

Analysis of RNA-seq data

Adapter sequences, reads of low quality ($Q \leq 20$) and those with ambiguous bases (multiple "N") were removed to obtain clean raw reads which were subsequently used for alignment with PGSC_DM_v6.1 gene models available at Solanaceae Genomics Resource at Michigan State University (http://solanaceae.plantbiology.msu.edu/pgsc_download.shtml)[68] using HISAT2 (v2.0.1). DESeq2 was then used for analyzing differentially expressed genes (DEGs) between two samples based on the raw counts, with an absolute value of $\log_2$FC ($\log_2$ fold change) > 1 and a false discovery rate (FDR) < 0.05 selected as thresholds to consider genes as being diffierentially expressed.[63] DEGs were then annotated against NR (Non-Redundant Protein Sequence Database), SwissProt/UniProt Plant Proteins, COG/KOG (Cluster of Orthologous Groups of proteins), Gene Ontology (GO) and KEGG. In this case, after enrichment analysis, p values <0.05 were taken as indicative of significantly enriched KEGG pathways and GO functions. The heatmap of gene expression profile was visualized by TBtools software.[65]

Module construction by analyzing co-expression networks

The "weighted gene co-expression network analysis (WGCNA)" package in R[44] was used and it allowed 20110 genes, with Fragments Per Kilobase of transcript per Million mapped reads (FPKM) values ≥ 2, to be identified from the 27 samples used for performing the co-expression network analysis. The eigengene values were calculated for each module to identify associated links with flavonoid compounds, with visualization of the interaction network conducted with Cytoscape v3.7.1 [44].

Construction of expression vectors

The whole coding sequences of *StMYB3* (Soltu.DM.05G004700) and *StMYBATV* (Soltu.DM.12G023200) were amplified using cDNAs as templates, which was obtained from the red flesh of R at the S3 stage as well as the following two pairs of designed primers: MYB3F: 5′- ATGAGAAAGCCTTGTTGTGATAACA-3′, MYB3R: 5′- CTATGGAAGTGAATTGAGATCAAGCAA-3′; MYBATVF: 5′- ATGGCTGATTTGGATAGTTCAAGCA-3′, MY BATVR: 5′- TTATTGGCTGGTGGAATTTCTTGAGT-3′. Gene amplification was achieved by PCR using Platinum Taq DNA Polymerase High Fidelity (Invitrogen, USA), with full-length fragments of both genes cloned into the plant expression vector pNC-Cam2304-MCS35S by nimble cloning.[63]

Transient assays to assess gene functions

Transient or dual-luciferase assays, were carried out in tobacco (*N. benthamiana* or *N. tabacum*).[69,70] For this assay, four different vectors were used: a pSAK277 vector containing StAN1-R1 and StbHLH1,[18] the pNC-Cam2304-MCS35S vector with StMYB3 and StMYBATV being under the control of the CaMV 35S promoter, a pGreenII 0800-LUC vector containing *prom-3-StDFR*, a promoter of the *DFR* gene in potato[18] and an empty vector which acted as the control. *Agrobacterium tumefaciens* strains GV3101 were then transformed with each of the above contructs. *Agrobacterium* cultures containing the reporter cassette and cassettes containing StMYB3/StMYBATV, StAN1-R1 and StbHLH1 were mixed with a ratio of 1:3:3:3 for infiltration experiments. *N. benthamiana* plants were grown in greenhouse until four to six leaves were available for infiltration with *Agrobacterium*. Approximately 300 μL of *Agrobacterium* culture containing genes of interest was infiltrated into a young leaf. At three days post infiltration, leaf discs were placed into a 96-well-plate containing 50 μL of PBS (PBS) with 4 replicates from each plant. LUC and REN activities were measured with a Varioskan Flash Multimode Microplate Reader (Thermo Fisher Scientific, USA).

In order to determine the functions of StMYB3 and StMYBATV, a separate color assay was performed using two-week-old seedlings of *N. tabacum*. Young leaves of the seedlings were injected with activated *Agrobacterium* cultures (OD_{600} = 0.8–1) consisting of either a mixture of equivalent doses of StAN1-R1 and StMYB3/StMYBATV, or StMYB3, StMYBATV alone. Meanwhile, *Agrobacterium* cultures containing *StMYB3* and empty vector were agroinfiltrated in fully expanded leaves of 2-week-old transgenic *N. tabacum* plants overexpressing the activator *StAN1-R1* as previously obtained (Liu et al.[18]). Photographs were taken seven days after the infiltration process.

Yeast two-hybrid assays

Full-length *StAN1*, *StMYB3*, and *StMYBATV* were cloned into pNC-GADT7, and *StbHLH1* was cloned into pNC-GBKT7. The combination of the indicated pNC-GADT7 (AD-EV, AD-*StAN1*, AD-*StMYB3*, and AD-*StMYBATV*) constructs with pNC-GBKT7 (BD-*StbHLH1*) was co-transformed into the AH109 yeast strain, and yeast cells were grown on -2SD (-Leu-Trp) medium for 5 days at 30°C. Transformed colonies were plated onto -4SD (-Leu-Trp-His-Ade) medium and grown at 30°C for 5 days to test the possible interactions. The plasmid combination of AD-*StAN1* and BD-*StbHLH1* was the positive control.

Bimolecular fluorescence complementation (BiFC) assays

In order to investigate *planta* interactions, BiFC assays were used to build constructs in the pNC-BiFC-Enn and pNC-BiFC-Ecn vectors.[63] The OFR of *StAN1*, *StMYB3*, *StMYBATV* were cloned into pNC-BiFC-Enn, and the *StbHLH1* was cloned into pNC-BiFC-Ecn. Electroporation was performed to transform these constructs into the *Agrobacterium* GV3101 strain (Primers list for plasmid synthesis in Table S1). Mixed *Agrobacterium* strains were used for infiltrating *N. benthamiana* leaves, with fluorescence signals detected at 488 nm using a confocal laser-scanning microscope (LSCM 800, Carl Zeiss, Germany) 48 h after infiltration.

Quantitative analysis of gene expression

For qRT-PCR analysis, eight genes related to tuber color were selected, with the primers listed in Table S1 and *StEF-1α* (AB061263) selected as a reference gene for template normalization.[71] SuperReal Pre-Mix Plus (SYBRGreen FP205; Tiangen, Beijing, China) was used as specified by the manufacturer and qPCR reactions were performed as follows: initial denaturation at 95°C for 15 min, followed by 40 cycles, each with denaturation at 95°C for 10 s and annealing at 60°C for 30 s. Finally, melting curve analysis was carried out in a

temperature range of 65–95°C. The standard curve of a cDNA serial dilution analyzed the qPCR efficiency. The quantitative data were calculated from triplicate samples using the comparative Ct ($2^{-\Delta\Delta Ct}$) method.

QUANTIFICATION AND STATISTICAL ANALYSIS

In the case of qPCR and dual luciferase promoter activation assays, data from four biological replicates were provided as means (±Standard Errors). Means were compared by one-way ANOVA and differences were tested for statistical significance using the least significant difference (LSD) at 5% significance level.